TFEB-Mediated Pro-inflammatory Response in Murine Macrophages Induced by Acute Alpha7 Nicotinic Receptor Activation

Havisha H. Honwad[1,2,6], Mehran Najibi[3], Balazs Koscso[4,5], Milena Bogunovic[4], and Javier E. Irazoqui[1*]

[1] Department of Microbiology, University of Massachusetts Chan Medical School, Worcester, USA

[2] Immunology & Microbiology Program, University of Massachusetts Chan Medical School, Worcester, USA

[3] Department of Pathology, New York University Grossman School of Medicine, New York, USA

[4] Department of Pathology, University of Massachusetts Chan Medical School, Worcester, USA

[5] Current address: Obsidian Therapeutics, Cambridge, USA

[6]Current address: Dana-Farber Cancer Institute, Harvard Medical School, Boston, USA

*Correspondence: Javier.Irazoqui@umassmed.edu

The authors declare no competing interests.

Abstract

Transcription factors TFEB and TFE3 are crucial for regulating autophagy, lysosomal biogenesis, and lipid metabolism, and have significant roles in macrophage function and innate immunity. The alpha7 nicotinic acetylcholine receptor (α7nAChR), a ligand-gated Ca^{2+} channel known for its therapeutic potential in neurological and inflammatory disorders, has been implicated in modulating immune responses by modulating macrophage function. Stimulation of α7nAChR with chemical agonists has been claimed to activate TFEB in pancreatic acinar cells and neurons. However, the impact of α7nAChR activation on TFEB and TFE3 in macrophages remained unknown, posing an important question due to the potential implications for inflammation regulation. This study investigates the effects of acute α7nAChR activation on TFEB-mediated responses in murine macrophages using the specific agonist PNU-282987. We demonstrate that α7nAChR stimulation triggers TFEB nuclear translocation and lysosomal expansion. Surprisingly, PNU-282987 induces a broad pro-inflammatory gene signature without concomitant cytokine secretion, suggesting an uncoupling of gene expression from cytokine release. Mechanistically, TFEB activation requires the lysosomal Ca^{2+} exporter MCOLN1 and the Ca^{2+}-dependent phosphatase PPP3/calcineurin. Additionally, PNU-282987 elevates reactive oxygen species (ROS) levels, and ROS are involved in TFEB activation by PNU-282987. Notably, even with α7nAChR deletion, compensatory ROS-mediated TFEB activation persists, suggesting the involvement of additional nicotinic receptors. Our findings reveal a novel α7nAChR-TFEB signaling axis in macrophages, offer new insights into the cholinergic regulation of

immune responses, establish a baseline for comparison with disease states, and identify potential therapeutic targets for modulating inflammation.

46 **Introduction**

47 Transcription factors of the Microphthalmia-TFE (MiT) family, including TFEB,
48 TFE3, MITF, and TFEC, are considered master regulators of autophagy and lysosomal
49 biogenesis [1]. In their resting state during homeostasis, TFEB and TFE3 reside in the
50 cytosol, where they are sequestered by 14-3-3. Under stressful conditions, such as
51 nutrient deprivation, TFEB and TFE3 localize to the nucleus, where they induce broad
52 transcriptional programs that include autophagy and lysosomal biogenesis genes. As a
53 result of TFEB and TFE3 activation, both autophagy and lysosomes are induced,
54 resulting in enhanced cellular clearance of protein aggregates and damaged organelles.
55 More recently, TFEB and TFE3 have also been shown to induce lipid catabolism [2, 3]
56 and to play important roles in the innate immune system [4, 5]. During phagocytosis of
57 bacteria or LPS stimulation, TFEB and TFE3 are activated in macrophages and required
58 for pro-inflammatory macrophage polarization [6, 7], indicating that TFEB can be an
59 important pro-inflammatory transcription factor in these cells. However, the roles and
60 regulation of TFEB and TFE3 in macrophage function are not yet well understood.

61 Upstream regulation of TFEB and TFE3 involves negative regulation by
62 mTORC1 under nutrient-replete conditions, mediated by phosphorylation [8, 9].
63 mTORC1 phosphorylation promotes 14-3-3 binding and cytosolic retention of TFEB and
64 TFE3 [8, 10, 11]. Dephosphorylation, mediated by Ca^{2+}-dependent protein phosphatase
65 3 (PPP3, calcineurin), lifts mTORC1-dependent repression of TFEB and TFE3 by
66 enabling their nuclear import [12]. In macrophages, phagocytosis of particles, such as
67 opsonized inert beads or bacterial cells, induces TFEB and TFE3 activation via this
68 mechanism. The Botelho, Kehrl, and our laboratories collectively revealed an upstream

69 pathway in macrophages that activates TFEB and TFE3 during phagocytosis, which
70 involves reactive oxygen species (ROS) production by NADPH oxidase, NAADP-
71 synthesizing enzyme CD38, NAADP-triggered Ca^{2+} release, lysosomal Ca^{2+} exporter
72 mucolipin 1 (MCOLN1), and calcineurin [6, 13, 14]. However, additional stimuli that
73 regulate macrophage function and impinge on TFEB and TFE3 are mostly unknown.

74 Nicotinic receptors (nAChRs) are pentameric ligand-gated Ca^{2+} channels, for
75 which the ligand is the neurotransmitter acetylcholine (ACh). Their subunit composition
76 varies by subtype, and may include α, β, γ, δ, and ε subunits. The α7nAChR is a
77 homopentameric assembly of type 7 α (α7) subunits, encoded in mice by gene *Chrna7*
78 [15]. Upon acute stimulation, the α7nAChR allows ionotropic Ca^{2+} entry and rapidly
79 desensitizes. However, longer stimulation can lead to metabotropic signaling due to
80 Ca^{2+}-induced Ca^{2+} release from intracellular stores [16]. Thus, persistent α7nAChR
81 stimulation is thought to activate downstream Ca^{2+}-dependent signaling pathways.

82 The α7nAChR has been long considered a therapeutic target for neurological
83 disorders including schizophrenia, and more recently attention has turned to its non-
84 neuronal functions. The α7nAChR is known to be expressed in many non-neuronal cell
85 types, including leukocytes, barrier epithelial cells, lung cancer cells, cardiomyocytes,
86 and vascular endothelial cells [17, 18]. Expression in macrophages is less well
87 documented, limited by the nonspecificity of affinity reagents and low levels of
88 expression that border on the limits of detection [18]. Nonetheless, considerable interest
89 in the immunomodulatory functions of the α7nAChR was fueled by the description of a
90 cholinergic cell circuit in the spleen, which represses NF-κB activity, systemic pro-
91 inflammatory cytokine production, and HMGB1 release during sepsis [19]. Several

92 agonistic small molecule compounds, including general agonist carbachol and
93 α7nAChR-specific PNU-282987, were shown to repress the production of pro-
94 inflammatory soluble mediators by phagocytes in *in vitro* and *in vivo* models of sepsis
95 [20]. However, the effects of these small molecules on resting macrophages have not
96 been addressed, leaving a gap in knowledge about the homeostatic functions of
97 α7nAChR that creates uncertainty about the clinical application of α7nAChR agonists as
98 anti-inflammatory drugs.

99 Recently, the α7nAChR was reported to activate TFEB in pancreatic acinar cells
100 and in a cellular model for amyotrophic lateral sclerosis (ALS) [21, 22]. The first report
101 showed that PNU-282987 induced Ca^{2+} influx and promoted TFEB nuclear localization,
102 lysosomal biogenesis, and autophagic flux in *in vitro* and *in vivo* models of acute
103 pancreatitis, but did not test the effects of α7nAChR stimulation in homeostasis or in
104 α7nAChR-deficient animals, define a pathway linking α7nAChR to TFEB, or define the
105 role of TFEB in the process [21]. The second report showed that PNU-282987 induced
106 TFEB nuclear localization dependent on Ca^{2+} and CAMKK in N2a neuronal cells
107 transfected with $SOD1^{G85R}$, which is causal for familial ALS [22]. In this case, PNU-
108 282987 induced known TFEB target genes, lysosomal biogenesis, and autophagy flux,
109 but again the role of TFEB was not defined and the effect of PNU-282987 on control
110 cells expressing wild type SOD1 was not addressed. Both studies ascribed the effects
111 of PNU-282987 to the α7NAChR, based solely on small molecule inhibitors. Thus, to
112 our knowledge whether α7nAChR stimulation activates TFEB in macrophages, and the
113 effects of such activation, remained an important gap in knowledge.

114 Here we report the results of our studies of the effects of α7nAChR stimulation in
115 several murine *in vitro* macrophage models. Our results show that stimulation of the
116 α7nAChR with PNU-282987 and other agents acutely triggers TFEB in murine
117 macrophages, which results in lysosomal expansion. The acute transcriptional response
118 to α7nAChR stimulation includes induction of a broad pro-inflammatory gene signature,
119 a large portion of which requires TFEB function. Paradoxically, this pro-inflammatory
120 gene signature is not accompanied by induced secretion of pro-inflammatory cytokines,
121 revealing an uncoupling of secretion from gene expression. Mechanistically, we show
122 that activation of TFEB and TFE3 requires MCOLN1, Ca^{2+}, and calcineurin function
123 downstream of α7nAChR. Moreover, we show that ROS accumulate in both PNU-
124 282987-treated and α7nAChR-deleted cells, revealing novel aspects of their
125 mechanisms of function that impact TFEB activation status. These results demonstrate
126 for the first time that the α7nAChR partially mediates the activation of TFEB
127 downstream of PNU-282987 in macrophages, and suggest the existence of additional
128 and unknown parallel pathways for TFEB activation that need to be elucidated.

129

130 **Results**

131 ***α7nAChR stimulation induces TFEB nuclear localization in macrophages***

132 To examine the effect of α7nAChR stimulation on TFEB, we used immortalized
133 BMDM (iBMDM) transduced to express GFP-tagged TFEB (GFP-TFEB) [7]. DMSO-
134 treated cells exhibited mainly cytosolic GFP-TFEB, es expected in resting cells (**Fig.**
135 **1A**). Cells treated with PNU-282987, an α7nAChR agonist [23], showed a marked

136 increase in nuclear GFP-TFEB (**Fig. 1B**), comparable to starved positive controls (**Fig.**
137 **1D, G**). Incubation with the cholinergic agent arecoline [24] also induced GFP-TFEB
138 nuclear localization (**Fig. 1C**). Thus, cholinergic stimulation and α7nAChR stimulation
139 both caused GFP-TFEB to localize to the nucleus. In contrast, α7nAChR inhibitor
140 MG624 abrogated these effects [25] (**Fig. 1E-G**). This result suggested that cholinergic
141 stimulation may activate TFEB through the α7nAChR.

142 To test that conclusion further, we used primary BMDMs, in which we visualized
143 endogenous TFEB by immunofluorescence. In these cells, TFEB signal is lower and
144 more diffuse than that of GFP-TFEB, owing to low TFEB expression and possibly to the
145 existence of several TFEB splice isoforms. Nonetheless, in resting cells TFEB
146 localization was predominantly cytosolic (**Fig. 1H**). As with iBMDM, arecoline and PNU-
147 282987 increased both TFEB nuclear localization and expression, as expected due to
148 TFEB auto-induction [3] (**Fig. 1I, J, N**). MG624 abrogated TFEB activation by arecoline
149 and by PNU-282987, suggesting that they acted through the α7nAChR. Carbachol is
150 another commonly used cholinergic agonist [26]. Carbachol treatment also activated
151 TFEB (**Fig. 1P, Q**), which was inhibited by MG624 (**Fig. 1S-U**). Thus, cholinergic and
152 α7nAChR stimulation activate TFEB in murine macrophages in an MG624-sensitive
153 manner.

154

155 ***α7nAChR stimulation activates lysosomes in macrophages***

156 When activated in the nucleus, TFEB drives lysosomal biogenesis, which is used
157 as a readout of TFEB activity [27]. To verify the biological significance of TFEB nuclear

158 translocation by cholinergic agents, we measured lysosomes by Lysotracker staining of
159 treated cells. Both carbachol and PNU-282987 caused increased Lysotracker staining
160 compared to vehicle controls (**Fig. 2B, C, I**) but less potently than mTOR inhibitor torin-1
161 and LPS, which strongly activate TFEB in macrophages (**Fig. 2D, E, J) [6, 28]**. MG624
162 suppressed lysosomal biogenesis induced by carbachol and PNU-282987 (**Fig. 2G, H,**
163 **I**). Moreover, MG624 reduced lysosomal staining in the vehicle controls, suggesting that
164 MG624 may repress lysosomes in resting macrophages. Together, these data suggest
165 that α7nAChR stimulation activates TFEB, increasing lysosomal biogenesis.

166

167 ***TFEB activation is likely not due to phagocytosis or cytotoxicity***

168 In macrophages, phagocytosis functions upstream of TFEB to drive its nuclear
169 localization [13]. To test phagocytosis as a mechanism for TFEB activation by
170 α7nAChR, we measured uptake and killing of *Escherichia coli* and *Staphylococcus*
171 *aureus*. In both infection models, carbachol and PNU-282987 had no effect on either
172 measure of macrophage function compared to vehicle controls (**Fig. S1A, B**). Therefore,
173 TFEB activation by carbachol and PNU-282987 is unlikely a result of increased
174 phagocytic activity and does not result in enhanced bacterial killing.

175 TFEB is known to be activated by diverse cellular stresses [29]]. To test
176 carbachol or PNU-282987 toxicity, we measured cell viability of treated BMDMs. Over a
177 128-fold concentration range, PNU-282987 and carbachol did not cause significant cell
178 death (**Fig. S1C, D**), confirming and extending previous results using murine peritoneal

179 macrophages [30] and murine macrophage-like cell line RAW264.7 [17]. These data
180 ruled out toxicity as a mechanism of TFEB activation by carbachol and PNU-282987.

181

182 ***PNU-282987 induces pro-inflammatory genes in macrophages***

183 To characterize the transcriptional effect of acute α7nAChR stimulation with PNU-
184 282987, we performed RNA-seq. Given the rapid kinetics of TFEB activation, we chose
185 to focus on an early treatment time that also yielded lysosomal expansion (2 h, **Fig. 2**)
186 to minimize secondary effects. Compared to vehicle control, PNU-282987 treatment
187 induced 572 induced genes and repressed 119 genes (**Fig. 3A, Table S1**). Surprisingly,
188 the induced genes were enriched for various KEGG pathways that were mostly related
189 to pro-inflammatory signaling (*e.g.* "TNF signaling pathway", "Cytokine-cytokine receptor
190 interaction", "NF-κB signaling pathway"), and "Lipid and atherosclerosis" (**Fig. 3B and**
191 **Table S2**). Complementary Gene Ontology (GO) and Reactome analyses also showed
192 enrichment of pro-inflammatory categories (**Fig. 3B and Table S2**). In contrast, the
193 repressed genes were not significantly enriched for any KEGG pathways or GO
194 categories. These results suggested that PNU-282987 induced a pro-inflammatory gene
195 expression profile in BMDMs.

196 To verify these results in an alternative *in vitro* model, we used RAW264.7 cells.
197 Similar to BMDMs, PNU-282987 induced a clear pro-inflammatory gene signature (**Fig.**
198 **3C, D and Table S3**). The induced pro-inflammatory gene categories (*e.g.* "Toll-like
199 receptor signaling pathway", "NOD-like receptor pathway", "NF-kappaB signaling
200 pathway", and "TNF signaling pathway", **Table S4**) included *Ifnb1, Il1b, Il6,* and *Tnf*, as

201 was the case with BMDMs. 240 genes were induced by PNU-282987 in both cell types;
202 these overlap genes were similarly enriched in pro-inflammatory genes of the same
203 categories as above (**Fig. 3E, F and Table S5**). Thus, in RAW264.7 cells as in BMDMs,
204 PNU-282987 treatment induced an early pro-inflammatory gene expression profile.

205 To test if the induced RNA expression resulted in cytokine secretion, we
206 performed ELISA of culture supernatants from BMDMs and RAW264.7 cells treated with
207 PNU-282987 for 12 h, to allow for protein production and secretion. PNU-282987
208 treatment did not induce the secretion of any of the cytokines IL-6, TNF-α, IFN-β1, IL-
209 1β, and IL-10 (**Fig. S2A-E**). PNU-282987 also did not cause measurable lactate
210 dehydrogenase (LDH) release (**Fig. S2F**), ruling out cell death as a reason for the lack
211 of cytokine secretion. Experiments with RAW264.7 cells essentially yielded the same
212 results (**Fig. S2G-K**). Thus, we concluded that PNU-282987 treatment did not increase
213 pro-inflammatory cytokine secretion despite inducing a strong pro-inflammatory gene
214 signature.

215 In contrast, PNU-282987 had a marked effect on cytokine secretion of LPS-
216 stimulated macrophages. After stimulation with LPS for 12 h, secretion of IL-6, TNF-α,
217 and IFN-β1 was elevated (**Fig. S2A-C**). Subsequent PNU-282987 treatment after LPS
218 stimulation strongly inhibited IL-6 secretion, but not that of TNF-α and IFN-β1 (**Fig. S2A-**
219 **C**). PNU-282987 treatment for 2 h prior to LPS stimulation only inhibited IL-6 (**Fig. S2A**).
220 These results showed that PNU-282987 inhibits LPS-stimulated IL-6 secretion under
221 both regimens. In parallel experiments with RAW264.7 cells, PNU-282987 treatment
222 prior to LPS stimulation inhibited IL-6, TNF-α, and IFN-β1, but treatment after LPS
223 stimulation did not (**Fig. S2G-K**). Thus, we confirmed and extended prior reports [17, 30]

224 showing that PNU-282987 prophylactically reduced LPS-induced IL-6 in murine
225 macrophages.

226

227 ***PNU-282987 induces pro-inflammatory genes via the α7nAChR***

228 To verify expression of α7nAChR, we followed several orthogonal approaches.
229 RT-qPCR using previously published [17, 31] and newly designed oligonucleotide
230 primers detected very low expression of nicotinic subunits α3 to α10 and β2 to β4, and
231 of muscarinic receptors M1 to M4 (**Table S6**). α7nAChR was not more highly expressed
232 than any other receptor subunit, except possibly M2. In contrast, *Chrna7* and *Chrnab2*
233 were readily detectable in RNA extracted from murine brains (**Table S6**). We also used
234 immunoblotting to detect α7nAChR in whole cell lysates using an anti-α7nAChR
235 antibody that was previously used for the same application [32, 33]. Whole-cell lysate
236 from WT BMDM did not show the putative α7nAChR band that was clearly visible in
237 mouse brain lysate, and there were no band differences between wild type and *Chrna7*
238 KO BMDMs (**Fig. S3A**). This result confirms the lack of specificity of commercially
239 available antibodies, as previously reported [34, 35]. We also used fluorescently
240 labelled α-bungarotoxin, a standard way to detect α7nAChR surface expression [36], in
241 primary tissue macrophages. Staining of primary murine macrophages from peritoneum,
242 ileum, and colon failed to detect α7nAChR expression (**Fig. S3B-I**). Finally, anti-
243 α7nAChR immunostaining and fluorescence microscopy did not show α7nAChR
244 expression (not shown). Thus, four orthogonal approaches and multiple macrophage
245 cell types did not detect, or barely detected, α7nAChR expression. α7nAChR
246 expression is known to be low and highly variable in leukocytes, with poor correlation of

247 mRNA and protein expression and lack of specific and sensitive tools to reliably detect
248 α7nAChR protein [18].

249 Therefore, we followed an alternative genetic approach to evaluate the role of
250 α7nAChR. Mice deleted for *Chrna7* were generated previously [37]. We used RNA-seq
251 to measure the PNU-282987-induced response in *Chrna7*$^{-/-}$ (*Chrna7* KO) BMDMs.
252 Compared to vehicle, PNU-282987 induced the expression of just 12 genes in *Chrna7*
253 KO BMDMs (**Fig. 4A and Table S7**), as opposed to 572 genes induced in the wild type
254 (**Fig. 3**). Notably, *Tnf* was still induced, as well as *Rragd* and *Fnip2*, which are mTOR
255 regulators and thus potentially upstream of TFEB. Moreover, only 8 genes were induced
256 in both wild type and *Chrna7* KO backgrounds (**Fig. 4B and Table S8**), supporting the
257 specificity of the PNU-282987 effect in terms of gene induction. Consistently, direct
258 comparison of PNU-282987-treated *Chrna7* KO BMDMs and wild type cells showed a
259 large defect in pro-inflammatory gene expression in the *Chrna7* KO BMDMs (**Fig. 4C, D**
260 **and Table S9**). The genes that were more highly expressed in PNU-282987-treated
261 *Chrna7* KO BMDMs were enriched in Ras and Rap1 signaling and lysosome categories,
262 suggesting compensatory pathways (**Table S10**). Thus, the induction of pro-
263 inflammatory genes by PNU-282987 is α7nAChR-dependent.

264 To better understand why *Chrna7* KO BMDMs exhibited such a strongly defective
265 response to PNU-282987, we examined expression of genes encoding macrophage
266 differentiation markers at baseline. Despite a few exceptions (CD11a, CD11c, CD14,
267 and MHC II), macrophage marker genes (CD15, CD16, CD64, CD32, F4/80, CD33,
268 CD68, CD80, and CD86) did not show significant differences between WT and *Chrna7*
269 KO BMDMs (**Fig. S4A, Table S11**) ruling out a broad defect in macrophage *in vitro*

270 differentiation. However, *Chrna7* KO BMDMs showed decreased expression of many
271 immune-related genes at baseline, such as *Il6, Il1a, Il1b, Cxcl2,* and *Nox1* (**Fig. S4B, C**
272 and **Table S12**), but also showed increased expression of other immune-related genes,
273 notably of the inflammatory response (**Fig. S4D** and **Table S13**). This result suggests
274 that deletion of α7nAChR has a non-neutral effect on immune gene expression of *in*
275 *vitro* differentiated BMDMs.

276

277 ***TFEB is required for the full transcriptional response to PNU-282987***

278 To define the effect of TFEB activation on the transcriptional response to PNU-
279 282987, we performed RNA-seq of conditionally TFEB-deleted BMDMs [6]. We
280 previously showed that TFEB expression is efficiently abrogated in this line [6]. At
281 baseline, the expression of a set of 23 macrophage differentiation markers was not
282 significantly different between *Tfeb*$^{fl/fl}$ and *Tfeb*$^{\Delta LysM}$ BMDMs, showing that *in vitro*
283 macrophage differentiation was not affected by *Tfeb* deletion (**Fig. S5A and Table S14**).
284 TFEB deletion decreased the expression of 665 genes compared to *Tfeb*$^{fl/fl}$ controls
285 (**Fig. S5B and Table S15**). Surprisingly, this gene set was not enriched for autophagy or
286 lysosomal genes, as might have been expected based on data from other cell types
287 [38]. Instead, this TFEB-dependent gene set was enriched in functional categories
288 related to “PI3K-Akt signaling”, “ECM-receptor interaction”, “Proteoglycans in cancer”,
289 and the extracellular matrix (**Fig. S5C and Table S16**). TFEB deletion also resulted in
290 higher expression of 138 genes (**Table S15**), but this gene set did not show significant
291 enrichment of functional categories. These results suggest that TFEB promotes the
292 expression of extracellular matrix genes in resting macrophages.

293 In PNU-282987-treated cells, deletion of TFEB resulted in decreased expression
294 of TNF-α signaling genes, in addition to the baseline defect in genes related to
295 extracellular matrix and PI3K-AKT compared to *Tfeb*$^{fl/fl}$ controls (**Fig. 5A, B and Tables**
296 **S17 and S18**). The genes that were more highly expressed in TFEB-deleted cells were
297 not enriched for any informative functional category. Thus, TFEB promotes the
298 expression of TNF signaling genes in response to PNU-282987.

299 Comparing the sets of genes that were induced by PNU-282987 in each genetic
300 background, deletion of TFEB abrogated the induction of 52 out of 118 total that were
301 induced in *Tfeb*$^{fl/fl}$ controls (**Fig. 5C and Table S19**). 19 additional genes were induced
302 only in TFEB-deleted cells. Thus, overall TFEB is required for about 40% of the
303 transcriptional response that is triggered by PNU-282987.

304 From these analyses in *Tfeb*$^{fl/fl}$, *Tfeb*$^{\Delta LysM}$, and wild type BMDMs, gene *Tnfsf15*
305 stood out as a PNU-282987-induced TFEB-dependent gene encoding a soluble
306 signaling mediator. Tumor necrosis factor superfamily-15 (TNFSF15), also called TL1A,
307 is a ligand for death receptor 3 (DR3), which activates signaling pathways involved in
308 immune cell activation, proliferation, apoptosis, and pro-inflammatory responses, and
309 thus could link PNU-282987 to proinflammatory gene expression [39]. To test if PNU-
310 282987-induced TNFSF15 production might cause macrophage activation, we
311 performed ELISA of supernatants from wild type and *Tfeb*$^{fl/fl}$ BMDMs. Treatment with
312 PNU-282987 did not increase soluble TNFSF15 under these conditions (**Fig. S5D**),
313 suggesting that TNFSF15 is not likely to be a mediator of PNU-282987-induced pro-
314 inflammatory gene expression.

315 To further test these conclusions, we used RAW264.7 cells that were deleted for
316 *Tfeb* and *Tfe3*, which encodes a TFEB paralog that heterodimerizes with TFEB but can
317 also function independently as a homodimer [40, 41]. In this model, PNU-282987-
318 treated *Tfeb Tfe3* double knockout (dKO) cells showed defective expression of 550
319 genes compared to wild type controls (**Fig. 5D and Table S20**). These genes were
320 enriched in pro-inflammatory pathways, notably TNF and NOD receptor signaling, as
321 well as lysosomal genes (**Fig. 5E and Table S21**), showing that TFEB and TFE3 are
322 important for the pro-inflammatory gene expression program that is triggered by PNU-
323 282987 in RAW264.7 cells. The genes that were more highly expressed in the *Tfeb*
324 *Tfe3* dKO cells did not show enrichment of any relevant functional categories. These
325 data strongly support the conclusion that PNU-282987 induces a pro-inflammatory gene
326 expression signature in a TFEB and TFE3-dependent manner.

327 Surprisingly, deletion of *Tfeb* and *Tfe3* abrogated IL-6 and IFN-β1 production
328 induced by LPS (but not that of TNF-α, **Fig. S6A-D**). Moreover, PNU-282987 induced 3-
329 fold higher LDH release in the *Tfeb Tfe3* dKO cells compared to WT (**Fig. S6E**),
330 suggesting that TFEB and TFE3 may mitigate PNU-282987 toxicity. However, at
331 baseline *Tfeb Tfe3* dKO cells showed decreased expression compared to wild type of
332 macrophage differentiation marker genes encoding CD11b, CD15, CD16, CD32, CD64,
333 CD33, and CD86, as well as TLR2 and TLR4 (**Fig. S6F, Tables S22 and 23**),
334 suggesting that the *Tfeb Tfe3* dKO cells may show an impaired macrophage phenotype.

335 Taken together, these data show that TFEB (and possibly TFE3) is an important
336 mediator of PNU-282987-induced gene transcription, but the upstream mechanism of
337 TFEB activation by PNU-282987 remained unknown.

338

339 ***The MCOLN1-Ca^{2+}-calcineurin pathway is important for α7nAChR stimulation of***
340 ***TFEB***

341 In previous studies, we showed that phagocytosis activates TFEB through a
342 pathway that involves ROS, Ca^{2+} release (potentially through the main lysosomal Ca^{2+}
343 pump MCOLN1), and protein phosphatase 3 (calcineurin), in that sequence [6]. To
344 examine the role of intracellular Ca^{2+} in PNU-282987-induced TFEB translocation, we
345 treated immortalized BMDMs expressing GFP-TFEB [6] with cell-permeable Ca^{2+}-
346 chelating agent BAPTA-AM prior to PNU-282987 treatment. BAPTA-AM pretreatment
347 suppressed the PNU-282987-induced nuclear localization of GFP-TFEB (**Fig. 6A-C, E**),
348 suggesting that intracellular Ca^{2+} is required for PNU-282987-induced TFEB nuclear
349 localization. Furthermore, pre-treatment with FK506, which inhibits calcineurin [42], also
350 prevented GFP-TFEB nuclear translocation (**Fig. 6D, E**), suggesting that PNU-282987-
351 induced intracellular Ca^{2+} functions through calcineurin to induce TFEB nuclear
352 translocation. In support of this conclusion, silencing of *Ppp3cb* and *Ppp3r1*,
353 respectively encoding catalytic and regulatory subunits of calcineurin, partially
354 suppressed PNU-282987-induced GFP-TFEB translocation (**Fig. 6F-I, M**). Likewise,
355 silencing of *Trpml1*, which encodes MCOLN1, also prevented GFP-TFEB translocation
356 by PNU-282987 (**Fig. 6K, M**), suggesting that Ca^{2+} export from the lysosome by
357 MCOLN1 is also required. Altogether, these results are consistent with PNU-282987-
358 induced activation of TFEB through the MCOLN1-Ca^{2+}-Calcineurin pathway.

359 In our previous research, we found that protein kinase D (PKD) 1 is required for
360 TFEB activation during bacterial infection and phagocytosis [7, 43]. To test the role of

361 PKD in PNU-282987-induced activation of TFEB, we used the PKD inhibitor kb-NB142-
362 70 [44]. Pretreatment of BMDMs with kb-NB142-70 suppressed TFEB translocation
363 caused by PNU-282987 (**Fig. S7**), thus implicating PKD in this mechanism of activation
364 as well.

365 We and others recently showed that oxidative stress and reactive oxygen
366 species can activate TFEB in macrophages and other cell types [6, 45, 46]. To test if
367 PNU-282987 induces ROS production, we used measured ROS levels in PNU-282987-
368 treated BMDMs. PNU-282987 induced the accumulation of both overall ROS and H_2O_2
369 specifically, which were suppressed by MG624 (**Fig**. **S8A, B**). MG624 alone also slightly
370 depressed H_2O_2 levels compared to vehicle controls. These results showed that PNU-
371 282987 induces ROS in BMDMs, which could be a mechanism for TFEB activation,
372 further implicating a ROS-MCOLN1-Ca^{2+}-calcineurin pathway. Suppression by MG624
373 is consistent with an α7nAChR-dependent mechanism.

374 At baseline, *Chrna7* KO BMDMs showed higher total ROS and H_2O_2 compared
375 to WT cells (**Fig. S8C, D**). The ROS and H_2O_2 levels in *Chrna7* KO BMDMs were similar
376 to those in PNU-282987-treated wild type BMDMs, and treatment with PNU-282987 did
377 not lead to further increases (**Fig. S8C, D**). Thus, both activation and loss of α7nAChR
378 led to increased ROS in macrophages.

379 To test the functional relevance to TFEB activation, we performed
380 immunofluorescence. In vehicle controls, *Chrna7* KO cells showed slightly less nuclear
381 TFEB than WT (**Fig. S8E**). PNU-282987 induced TFEB translocation in both genotypes,
382 but to a lesser degree in *Chrna7* KO cells, suggesting both α7nAChR-dependent and
383 independent mechanisms of activation (**Fig. S8E**). Pre-incubation with N-acetyl L-

384 cysteine (NAC), a ROS scavenger, reduced TFEB nuclear localization in both genetic
385 backgrounds, as also did FK506, BAPTA-AM, and MCOLN1 inhibitor ML-SI3 [47] (**Fig.**
386 **S8F, G**). Thus, ROS scavenging and inhibition of Ca^{2+}, MCOLN1, and calcineurin all
387 suppressed TFEB nuclear translocation induced by PNU-282987 even in α7nAChR-
388 deleted cells. These results suggest both α7nAChR-dependent and -independent
389 mechanisms of TFEB activation by PNU-282987 and, possibly, other α7nAChR
390 agonists.

391

392 **Discussion**

393 For our studies, we focused on resting cell lines and primary macrophages.
394 Resting, or naïve, macrophages are crucial for preserving tissue homeostasis and
395 performing routine clearance of apoptotic cells and debris, ensuring immune
396 surveillance without initiating inflammatory responses [48, 49]. In naive macrophages,
397 we can assess baseline cellular responses to α7nAChR agonists without the
398 confounding effects of prior activation, allowing for a clearer distinction of the direct
399 effects of these agonists on macrophage function [50, 51]. Establishing a baseline with
400 naive macrophages enables comparative studies with activated macrophages,
401 elucidating how α7nAChR might modulate functions in different activation states [52].
402 Furthermore, naïve macrophages can help us understand how early interventions with
403 α7nAChR agonists might modulate the immune system before inflammation or infection
404 onset, providing insights into designing preventative therapies that maintain immune
405 homeostasis [53]. Understanding the role of naïve macrophages in tissue repair and
406 regeneration offers insights into their potential therapeutic roles in preventing or

407 mitigating chronic inflammatory diseases such as atherosclerosis and fibrosis [54].
408 Thus, studying naïve macrophages is essential for a comprehensive understanding of
409 the endogenous functions of α7nAChR and of the therapeutic potential of α7nAChR
410 agonists.

411 Our results show that cholinergic agonists, both nonspecific (arecoline and
412 carbachol) and specific for α7nAChR (PNU-282987), activate TFEB and lysosomal
413 biogenesis in various macrophage models, including RAW264.7, immortalized BMDMs,
414 and primary BMDMs. Therefore, TFEB is a novel mediator of cholinergic signaling in
415 these important cells of the innate immune system. TFEB activation by these agonists is
416 suppressed by α7nAChR-specific antagonist MG624, suggesting that most of the effect
417 is α7nAChR-mediated. However, deletion of α7nAChR reduced but did not abrogate the
418 activation of TFEB by its agonist, suggesting that there may be a second mechanism
419 downstream of PNU-282987 that is also MG624-sensitive. The identity of this second
420 mechanism is currently unknown, but we speculate that it could involve an additional
421 nicotinic receptor that may also be inhibited by MG624. RAW264.7 cells were recently
422 reported to express several nicotinic receptor α subunits (3 to 7, 9, and 10) and β
423 subunits (2 to 4) [55], but more data are required to support this speculation.
424 Nonetheless, an independent study using α7nAChR agonist GTS-21 in peritoneal
425 macrophages reached similar conclusions [56].

426 Nonetheless, α7nAChR deletion almost completely abrogated the transcriptional
427 response to PNU-282987 stimulation, consistent with the majority of the signaling
428 downstream to be mediated through the α7nAChR. By comparison, TFEB deletion
429 eliminated about 40% of the transcriptional response, showing the biological relevance

430 of TFEB activation and suggesting that transcription factors other than TFEB are
431 involved. Although their identity remains unknown, it is tempting to speculate that an
432 additional Ca^{2+}-regulated transcription factor may provide that function. However, our
433 demonstration that modulating α7nAChR activity through agonism and deletion
434 increases ROS and triggers the MCOLN1-Ca^{2+}-calcineurin pathway adds a new
435 element to consider for signaling downstream of α7nAChR. This is consistent with prior
436 reports that showed that nicotine induces ROS production in RAW264.7 cells [57]. Thus,
437 it is also possible that a redox-sensitive transcription factor may be involved in parallel
438 to TFEB. Further work to elucidate these scenarios is merited.

439 Transcriptionally, we find that engaging α7nAChR through PNU-282987 induces
440 a pro-inflammatory response that does not translate into cytokine production by the
441 times that we evaluated. This is surprising for two reasons. First, a large body of
442 literature documents the anti-inflammatory effects of α7nAChR activation with PNU-
443 282987 and other agonists. Indeed, our data recapitulate some of these findings in
444 macrophages that are stimulated with LPS. In their resting state, however, the same
445 macrophages respond by inducing a slew of pro-inflammatory genes in a partially
446 TFEB-dependent manner. This result confirms and extends prior reports of pro-
447 inflammatory responses induced by nicotine in murine RAW264.7 cells and peritoneal
448 macrophages, as well as the aggravation of atherosclerosis *in vivo* [58]. Additionally,
449 many reports document pro-inflammatory activities of nicotinic agonists. Nicotine also
450 induces the production of PGE2, a product of COX-1 and COX-2 induced during
451 inflammation, in primary human monocytes [59, 60], induces the production of CRP by
452 U937 human monocytes [61], induces IL-6 in human monocytic THP-1 cells [62], and at

453 low concentrations potentiates the ATP-induced inflammatory response in rat primary
454 microglial cells [63]. Moreover, treatment of human THP-1 and monocyte-derived
455 macrophages with PNU-282987 induced an activated phenotype and was proposed as
456 an anti-immunosuppression strategy [64]. The exact reasons behind these divergent
457 behaviors are currently unclear. One possibility is that after the initial pro-inflammatory
458 phase, the transcriptome settles to a refractory or less responsive state perhaps through
459 epigenetic mechanisms. Indeed, most reports evaluated PNU-282987 and similar
460 agents on longer time scales than we did, because of our experimental focus on primary
461 transcriptional events that are relevant to the time scale of TFEB activation. Longer
462 stimulation times raise concerns about secondary effects [18].

463 The second reason for surprise is that the strong pro-inflammatory gene
464 signature does not result in concomitant cytokine production. However, this observation
465 is not without precedent. Cytokine expression is subjected to multiple layers of post-
466 transcriptional control [65, 66]. Moreover, in the case of IL-1β, TLR signaling provides
467 signal 1 to induce its transcription, while the NLRP3 inflammasome provides signal 2 to
468 induce its maturation and secretion through gasdermin-generated membrane pores [67,
469 68]. Thus, the lack of cytokine production in the supernatants of PNU-282987 cells
470 could be evidence of post-transcriptional control or of necessary but absent co-signals.
471 This “poised” state may help pro-inflammatory responses when signal 2 is presented.
472 Further investigation of this mechanism could offer new insight into the physiological
473 regulation of inflammation.

474 Although sometimes useful as probes and as proof of concept for therapeutic
475 strategies, small molecules like PNU-282987 fall short of fully recapitulating the

476 endogenous ligand, in this case the neurotransmitter acetylcholine. *In vivo*, the role of
477 TFEB as mediator of acetylcholine signaling is likely to be much more complex. In future
478 research, it will be important to disentangle the cellular sources of acetylcholine, the
479 cellular targets that express receptors capable of engaging TFEB, and the physiological
480 importance of these interactions within the innate immune system and beyond.

481

482 **Materials and Methods**

483 ***Mice***

484 Mouse colony maintenance and procedures were performed following the
485 Guidelines for the Care and Use of Laboratory Animals, published by the US National
486 Institutes of Health, and were approved by the Institutional Animal Care and Use
487 Committee (IACUC) of the University of Massachusetts Chan Medical School. Wild type
488 mice, strain C57BL/6J (Stock #: 000664) and *Chrna7*$^{-/-}$ mice, strain B6. 129S7-
489 *Chrna7*$^{tm1Bay/J}$ (Stock #: 003232) were from The Jackson Laboratory. *Tfeb*$^{fl/fl}$ mice were a
490 gift from Dr. Andrea Ballabio, TIGEM, Naples, Italy [69]. *Tfeb*$^{fl/fl}$ *LysM-Cre* mice were
491 bred in-house [6]. BMDM genotyping for wild type and *Chrna7*$^{-/-}$ BMDMs was performed
492 by Protocol 28408: Standard PCR Assay - Chrna7<tm1Bay>-Alternate 1 for Jackson lab
493 stock No. 003232.

494 ***Isolation and differentiation of primary murine BMDMs***

495 Bone marrow cells were isolated from separated femurs and tibias from
496 euthanized 8 to 12-week-old mice as previously described [6]. Isolated bone marrow
497 cells from C57BL/6, *Chrna7*$^{-/-}$, *Tfeb*$^{fl/fl}$ and *Tfeb*$^{\Delta LysM}$ mice were cultured in BMDM

498 differentiation medium: DMEM containing 4.5 g/L glucose, L-glutamine (Corning, 10-
499 013-CV), sodium pyruvate supplemented with 20% conditioned medium from L929
500 cells, 10% FBS, 1% AA for 7 days. Cells were seeded in non-tissue culture treated Petri
501 dishes (Fisherbrand, FB0875712) and incubated at 37°C, in a humidified chamber with
502 5% CO_2. Cells were seeded for experiments after 7 days of differentiation.

503 ***Cell culture and transfection***

504 G418 sulfate (Life Technologies, 10131) was used for selection. RAW264.7 and
505 *Tfeb*$^{-/-}$ *Tfe3*$^{-/-}$ RAW264.7 cells, a gift from Dr. Rosa Puertollano, NHLBI [5], and iBMDMs
506 [6] were grown in Dulbecco's Modified Eagle's Medium (DMEM) containing 4.5 g/L
507 glucose, L-glutamine (Corning, 10-013-CV), sodium pyruvate supplemented with 10%
508 Fetal Bovine Serum (FBS; Gibco, 16000044) and 1% Antibiotic-Antimycotic (Gibco,
509 15240062). Cells were grown at 37 °C, in a humidified chamber with 5% CO_2 and
510 passaged 4 to 10 times.

511 ***Drugs and Reagents***

512 PNU-282987 (Sigma-Aldrich, P6499) powder was dissolved in DMSO (Sigma-
513 Aldrich, D2438) - sterile, filtered, cell culture grade, Bio Performance certified, meets EP
514 and USP specifications and thus devoid of endotoxin or pro-inflammatory contaminants;
515 Carbachol (Sigma-Aldrich, 212385); MG624 (Cayman Chemical Company, 24298);
516 Arecoline (Cayman Chemical Company, 13662); LPS from *S. enterica* serotype
517 Typhimurium (Sigma-Aldrich, L6143-1 MG); Torin-1 (Tocris, 427); FK-506 (Cayman
518 Chemical Company, 10,007,965); BAPTA-AM (Cayman Chemical Company, 15,551);
519 kb-NB-142-70 (Cayman Chemical Company, 18,002); ML-SI3 was a gift from Drs. Juan

520 Marugán and Raúl Clavo of the National Center for Advancing Translational Science of
521 the National Institutes of Health (NCATS/NIH); α-bungarotoxin Alexa Fluor 647
522 conjugate (Thermo Fisher Scientific, B35450).

523 ***Immunofluorescence and fluorescence imaging***

524 Cells were seeded in 96-Well Optical Bottom Plates (Thermo Scientific, 165305)
525 and incubated overnight to attain cell confluency of 0.06 x 10^6 for experiments.
526 Following experiments, cells were fixed using 4% paraformaldehyde (PFA) (Sigma
527 Aldrich, 158127) and incubated with Hoechst stain (Anaspec, AS-83218) for 20 min at
528 room temperature. For immunofluorescence, cells were washed 3 times with PBS
529 (Gibco Life Technologies,10010) for 5 min, permeabilized with 0.1% Triton X in PBS
530 with shaking at room temperature for 5 min, washed 3 times with PBS and blocked with
531 5% bovine serum albumin (Sigma Aldrich, A9647) in PBS for 1 h. After washing with
532 PBS (3 times), cells were incubated with primary goat anti-TFEB antibody (Abcam,
533 ab2636) for 2 h. After washing 3 times in PBS, cells were incubated with donkey anti-
534 goat IgG -Alexa 594 secondary antibody (Thermo Fisher Scientific, A11058) along with
535 Hoechst stain (Anaspec, AS-83,218) for 1 h at room temperature. For LysoTracker
536 staining, cells were incubated with 100 nM LysoTracker DND-99 (Thermo Fisher,
537 L7528) added to cell culture media 30 min before fixation step, according to
538 manufacturer's instructions. Image acquisition for calculating TFEB N:C ratio and for
539 Lysotracker mean fluorescence intensity (MFI) was performed using Lionheart FX
540 automated microscope (Biotek) and Gen5 software (version 3.13).

541 ***Determination of N:C ratio***

542 Nucleus to cytoplasm (N:C) ratio for TFEB was measured using CellPofiler [70],
543 following our previously described protocol [6]. In brief, we used the
544 3_channels_pipeline.cppipe. algorithm, which uses nuclear stain (Hoechst) as primary
545 object or “seed” region for building image segmentation masks to distinguish individual
546 cells by marking boundaries, define subcellular regions and generate specific
547 fluorescent intensity values. The pipeline calculated N:C ratio as mean fluorescent
548 intensity of nucleus relative to mean fluorescence intensity of the region defined as
549 cytosol.

550 ***RT-qPCR***

551 Cells were lysed using Trizol Reagent (1 mL per 1.5 ml microcentrifuge tube).
552 100 µL chloroform was added and samples were centrifuged at 12,000 rpm to separate
553 the RNA containing aqueous phase. The aqueous layer was transferred to Purelink
554 RNA mini kit column and total RNA was extracted according to manufacturer’s
555 instructions. cDNA was prepared using iScript gDNA clear cDNA synthesis kit (Bio-Rad,
556 1725035). Diluted cDNA was used for RT-qPCR, performed using SYBR Green Super
557 mix (Bio-Rad) and ViiA7 Real-Time qPCR system (Applied Bioscience). Ct values were
558 obtained for test genes and relative expression was plotted following normalization to
559 reference gene *Gapdh*. Oligonucleotide sequences are included in **Table S24**.

560 ***RNA sequencing and differential expression analysis***

561 BMDMs differentiated from WT, *Chrna7*$^{-/-}$, *Tfeb*$^{fl/fl}$, *Tfeb*$^{\Delta LysM}$ mice were treated
562 with DMSO control or PNU-282987 (50 µL) for 2 h. Total RNA was extracted from
563 samples as described above using Purelink RNA mini kit (Thermo Fisher Scientific,

564 12183018A). PolyA selection, library preparation and sequencing using Illumina Nova-
565 Seq or HiSeq platform, 2x150bp, ~350,000,000 paired-end reads was performed from
566 whole cell RNA from 4 replicates per condition by Azenta/Genewiz. Azenta/Genewiz
567 provided raw data in the form of reads in FASTQ format. FASTQ files were analyzed
568 using the RNA-seq pipeline (v1.6.0) on ViaFoundry Inc. software (v1.6.5), which is
569 derived from DolphinNext [71]. Using the pipeline, FASTQ paired end reads were
570 trimmed, quality filtered by FastQC, followed by 3' adapter sequence removal and
571 aligned to *Mus musculus* reference genome mm10 using STAR, and RSEM was used to
572 estimate gene and isoform expression levels. DEBrowser (v1.28.0) was used for gene
573 count normalization, data analyses, and to generate visual graphs of differentially
574 expressed genes [72]. Differentially expressed gene sets were considered significant for
575 fold change ≥ 1.5; Padj ≤ 0.01 and were used as input for g:Profiler [73]. Comparison of
576 DE genes with public GEO RNA-Seq datasets was performed using Enrichr [74]. Venn
577 diagrams were made using DeepVenn [75].

578 ***ELISA***

579 Secreted TNF-α (DY410-05), IL-1β (DY401-05), IL-6 (DY406-05), IFN-β
580 (DY8234-05), IL-10 (DY417-05), TNFSF15 (DY-1896) were measured using ELISA kits
581 purchased from R&D Systems. Briefly, 96-well plates were coated with capture antibody
582 and incubated at room temperature overnight. Plates were washed with Tris buffered
583 saline (TBS) with 0.5% Tween 20 (Bethyl Laboratories, E106). Wells were blocked for 1
584 h with Reagent Diluent - TBS containing 1% bovine serum albumin (BSA) (Bethyl
585 Laboratories, E106). After washing, samples or standards diluted in Reagent Diluent
586 were added and plates were incubated for 2 h at room temperature. Detection antibody

587 was added following washing and plates were incubated for 2 h. After washing,
588 Streptavidin-horseradish peroxidase (Strep-HRP) was added for 20 min. TMB One
589 Component HRP Microwell substrate (Bethyl Lab, E102) was added, and reaction was
590 stopped using ELISA Stop Solution (Bethly Laboratories, E115). Optical density (OD) at
591 450 nm and 540 nm was measured immediately using a SpectraMax Plus 384
592 Microplate Reader with Softmax Pro software. OD measured at 540 nm was subtracted
593 from 450 nm to correct for optical imperfections as per manufacturer's guidelines.
594 Concentrations of the samples were interpolated from respective standard curves using
595 GraphPad Prism 10.

596 ***Cell viability assay***

597 Cell viability was determined using CellTiter-Glo 2.0 Assay (Promega, G7570),
598 according to the manufacturer's instructions. Luminescence was measured using Biotek
599 Synergy H4 Plate Reader Gen5 (version 3.14).

600 ***ROS/Superoxide detection assay***

601 Cellular ROS/Superoxide Detection Assay Kit (Abcam, ab139476) was used
602 according to manufacturer's instructions. Mean fluorescence intensity (MFI) was
603 visualized on a Lionheart microscope (Biotek) and measured using Gen5 Data Analysis
604 Software (Version 3.13).

605 ***siRNA knockdown***

606 siRNA reagents were purchased from Dharmacon RNAi Technologies:
607 siGENOME NonTargeting siRNA #1 (D-001210-01-05), siGENOME Mouse Ppp3cb
608 (19,056) siRNA (M-063545-00-0005), siGENOME Mouse Ppp3r1 (19,058) siRNA (M-

609 040744-01-0005), siGENOME Mouse Mcoln1 (94178) siRNA (M-044469-00-515 0005).
610 For transfection, we used Lipofectamine RNAiMAX (Thermo Scientific, 13,778,030),
611 according to manufacturer's instructions.

612 ***Western Blotting***

613 Cell samples were washed 3 times with PBS, harvested, and lysed with 1X SDS
614 sample buffer Blue Loading Pack (Cell Signaling Technology, 7722) at 100 µl per well of
615 6-well plate. Lysates were heated at 100 °C for 5 min and then centrifuged for 5 min.
616 Supernatants were collected and sonicated, followed by gel electrophoresis using
617 polyacrylamide Novex 4–20% Tris-Glycine Mini Gels (Invitrogen, XP04200BOX), and
618 transfer onto nitrocellulose (Life Technologies, LC2009). After washing with TBS (Life
619 Technologies, 28,358) for 5 min, membranes were soaked in blocking buffer containing
620 1X TBS with 5% BSA for 1 h at room temperature. After 3 washes with TBS-Tween 20
621 (Life Technologies, 28,360), membranes were incubated overnight at 4°C with primary
622 antibodies and gentle agitation. Next, membranes were washed thrice with TBS-Tween
623 20 and incubated with HRP-conjugated secondary antibody (Cell Signaling Technology,
624 7074 1:2000) for 1 h at room temperature with gentle agitation. Membranes were then
625 washed with TBS-Tween20 and incubated with LumiGLO® (Cell Signaling Technology,
626 7003) for 1 min and imaged using Gel box imager (Syngene) GeneSys software.
627 Primary antibodies and dilutions were as follows: ACTB/β-actin antibody (Cell Signaling
628 Technology, 4967; 1:1000), α7nAChR antibody (Abcam ab216485, 1:500).

629 ***α-bungarotoxin staining and flow cytometry***

630 α-bungarotoxin, Alexa Fluor 647 Conjugate (Thermo Fisher Scientific, B35450)
631 was used according to manufacturer's guidelines to stain murine peritoneal
632 macrophages and muscularis macrophages, isolated according to previously described
633 methods [76] by flow cytometry-based cell sorting [77]. Data were analyzed with
634 FlowJo.

635 ***Mouse whole brain lysate for Western Blot***

636 Frozen brain tissue from adult 9-month-old C57Bl/6J mice were homogenized in
637 ProcartaPlex™ Cell Lysis Buffer (ThermoFisher #EPX-99999-000) and centrifuged at
638 4°C for 20 min at 18000 x g.

639 ***Determination of bactericidal activity***

640 *Escherichia coli* DH5α was purchased from ThermoFisher Scientific (18265017).
641 *Staphylococcus aureus* NCTC8325 is a gift from Fred Ausubel, MGH Research
642 Institute, USA. Bacteria were grown overnight at 37°C in TSB (Sigma-Aldrich, T8907)
643 supplemented with 10 µg/ml nalidixic acid for *S. aureus*, or LB medium (Fisher
644 Scientific, BP1425-500) for *E. coli*. Cultures were diluted 1:50 in the respective media
645 the next day and grown at 37°C to mid-exponential phase. WT and *Tfe3 Tfeb* dKO RAW
646 264.7 cells were infected with *S. aureus* (MOI = 10) or *E. coli* (MOI = 50) and incubated
647 at 37°C for 30 min as previously described [6]. Lysates were serially diluted, aliquots
648 plated on TSA (Difco, BD, 236,950)-nalidixic acid agar (*S. aureus*) or LB agar (*E. coli*)
649 and incubated overnight at 37°C, and colonies were counted for colony-forming units/ml
650 calculation.

651 ***Statistical analysis***

652 Quantitative data comparisons were analyzed using statistical tests, performed
653 as indicated in each figure legend. $P \leq 0.05$ were judged to be significant. For normally
654 distributed data and comparisons with a single condition, we used the two-sample two-
655 sided *t*-test. For multiple comparisons, we used one-way ANOVA followed by Tukey's
656 *post-hoc* test and two-way ANOVA with Šídák's multiple comparisons test.

657

658 **Acknowledgments**

659 We thank the members of the Irazoqui Lab, Department of Microbiological and
660 Physiological System (MaPS), Department of Pathology, and the Immunology and
661 Microbiology Graduate Program (IMP) for helpful feedback and insights. Dr. Alper
662 Kucukural and Dr. Onur Yukselen provided help with RNA-sequencing data analysis
663 tools. Nicole Briand provided expert technical assistance. Thuyvan Luu and Abigail
664 Hiller from Dr. Paul Greer's Lab (UMCMS) provided mouse whole brain lysate samples
665 and whole brain lysate cDNA. Amy Parker, Annette Bohigian, Richard Fish, Tracey Rae,
666 Dhruti Desai, and Marie Berardi provided excellent administrative support. This work
667 was supported by the National Institute of General Medical Sciences of the National
668 Institutes of Health under award numbers R01GM101056 and R35GM149284 (JEI), and
669 by the Dr. Marcellette G. Williams Memorial Fund (JEI). The content is solely the
670 responsibility of the authors and does not necessarily represent the official views of the
671 National Institutes of Health.

672

673 **Figure Legends**

674 ***Figure 1. α7nAChR agonism activates TFEB in macrophages***

675 **A-F.** Representative fluorescence micrographs of GFP-TFEB iBMDMs treated
676 with DMSO (negative control) (**A**), PNU-282987 (50 μM, 2 h) (**B**), arecoline (1 μM, 2 h)
677 (**C**), serum starvation (positive control, 2 h) (**D**), MG624 (1 μM, 2 h pre-treatment)
678 followed by addition of PNU-282987 (50 μM, 2 h) (**E**), or MG624 (1 μM, 2 h pre-
679 treatment) followed by addition of arecoline (1 μM, 2 h) (**F**).

680 **G.** Quantification of A-F. Nucleus to cytoplasmic (N/C) ratio of GFP-TFEB (400
681 cells per condition, 3 biological replicates, ****$p \leq 0.0001$, one-way ANOVA followed by
682 Tukey's post-hoc test).

683 **H-M.** Representative immunofluorescence micrographs of WT BMDMs stained
684 with anti-TFEB antibody, treated with DMSO (**H**), arecoline (1 μM, 2 h) (**I**), PNU-282987
685 (50 μM, 2 h) (**J**), MG624 (1 μM, 2 h) (**K**), MG624 (1 μM, 2 h pre-treatment) followed by
686 addition of arecoline (1 μM, 2 h) (**L**), or MG624 (1 μM, 2 h pre-treatment) followed by
687 addition of PNU-282987 (50 μM, 2 h) (**M**).

688 **N.** Quantification of H-M. N/C ratio of TFEB in BMDMs (400 cells per condition,
689 **$p \leq 0.01$, ****$p \leq 0.0001$, one-way ANOVA followed by Tukey's post-hoc test).

690 **O-T.** Representative immunofluorescence micrographs of WT BMDMs stained
691 with anti-TFEB antibody, treated with DMSO (**O**), carbachol (50 μM, 2 h) (**P**), carbachol
692 (100 μM, 2 h) (**Q**), MG624 (1 μM, 2 h) (**R**), MG624 (1 μM, 2 h pre-treatment) followed by
693 addition of carbachol (50 μM, 2 h) (**S**), or MG624 (1 μM, 2 h pre-treatment) followed by
694 addition of carbachol (100 μM, 2 h) (**T**).

695 **U.** Quantification of O-T. N/C ratio of TFEB in BMDMs (400 cells per condition,
696 $^{**}p \leq 0.01$, $^{****}p \leq 0.0001$, one-way ANOVA followed by Tukey's post-hoc test).

697

698 ***Figure 2. α7nAChR agonism induces lysosomes in macrophages***

699 **A-H.** LysoTracker staining of GFP-TFEB iBMDMs treated with DMSO (**A**), PNU-
700 282987 (50 μM, 2 h) (**B**), Carbachol (50 μM, 2 h) (**C**), LPS (positive control, 100 ng/mL,
701 2 h) (**D**), Torin-1 (positive control, 1.25 μM, 1 h) (**E**), MG624 (1 μM, 2 h) (**F**), MG624 (1
702 μM, 2 h pre-treatment) followed by addition of carbachol (50 μM, 2 h) (**G**), or MG624 (1
703 μM, 2 h pre-treatment) followed by addition of PNU-282987 (50 μM, 2 h).

704 **I.** Quantification of A-C, F-H. LysoTracker mean fluorescence intensity (MFI) per
705 cell. 3 biological replicates (400 cells per condition, $^{****}p \leq 0.0001$, one-way ANOVA
706 followed by Tukey's post-hoc test).

707 **J.** Quantification of D and E. LysoTracker MFI per cell. 3 biological replicates
708 (400 cells per condition, $^{****}p \leq 0.0001$, one-way ANOVA followed by Tukey's post-hoc
709 test).

710

711 ***Figure 3. α7nAChR agonism acutely induces pro-inflammatory genes in***
712 ***macrophages***

713 **A.** RNA-seq of wild type (WT) BMDMs treated with PNU-282987 (50 μM, 2 h) v.
714 DMSO controls (fold change (FC) ≥ 1.5; *P*adj. ≤ 0.01, 4 biological replicates). Red

715 indicates upregulated (UP), blue denotes downregulated (DOWN) genes in PNU-
716 282987-treated cells. Notable pro-inflammatory and other genes are highlighted.

717 **B.** Gene ontology (GO) over-representation and KEGG pathway enrichment
718 analysis for PNU-282987-induced genes in A.

719 **C.** RNA-seq of WT RAW264.7 cells treated with PNU-282987 (50 μM, 2 h) v.
720 DMSO controls (FC ≥ 1.5; *P*adj. ≤ 0.01). Red indicates upregulated (UP), blue denotes
721 downregulated (DOWN) genes in PNU-282987-treated cells. Notable pro-inflammatory
722 and other genes are highlighted.

723 **D.** GO over-representation and KEGG pathway enrichment analysis of PNU-
724 282987-induced genes in C.

725 **E.** Overlap between PNU-282987-induced genes in RAW264.7 cells and
726 BMDMs.

727 **F.** GO over-representation and KEGG pathway enrichment analysis of overlap
728 PNU-282987-induced genes in E.

729

730 ***Figure 4. α7nAChR is required for the pro-inflammatory transcriptional response***
731 ***to PNU-282987.***

732 **A.** RNA-seq of *Chrna7*$^{-/-}$ BMDMs treated with PNU-282987 (50 μM, 2 h) v. DMSO
733 controls (FC ≥ 1.5; *P*adj. ≤ 0.01, 4 biological replicates). Red indicates upregulated
734 (UP), blue denotes downregulated (DOWN) genes in PNU-282987-treated cells.
735 Notable genes are highlighted.

736 **B.** Overlap of genes induced by PNU-282987 in WT (from Fig. 3A) compared to
737 those induced in *Chrna7*$^{-/-}$ BMDMs.

738 **C.** Differential gene expression of PNU-282987-treated (50 μM, 2 h) WT and
739 *Chrna7*$^{-/-}$ BMDMs (FC ≥ 1.5; *P*adj. ≤ 0.01, 4 biological replicates). Red indicates
740 upregulated (UP), blue denotes downregulated (DOWN) genes in *Chrna7*$^{-/-}$ cells.
741 Notable genes are highlighted.

742 **D.** GO-overrepresentation and KEGG pathway enrichment analysis for genes
743 upregulated in PNU-282987-treated WT BMDMs compared to *Chrna7*$^{-/-}$.

744

745 ***Figure 5. TFEB is required for a large fraction of the transcriptional response to***
746 ***PNU-282987***

747 **A.** Differential gene expression of PNU-282987-treated (50 μM, 2 h) *Tfeb*$^{f/f}$ and
748 *Tfeb*$^{\Delta LysM}$ BMDMs (FC ≥ 1.5; *P*adj. ≤ 0.01, 4 biological replicates). Red indicates
749 upregulated (UP), blue denotes downregulated (DOWN) genes in *Chrna7*$^{-/-}$ cells.
750 Notable genes are highlighted.

751 **B.** GO-overrepresentation and KEGG pathway enrichment analysis for genes
752 upregulated in PNU-282987-treated *Tfeb*$^{f/f}$ BMDMs compared to *Tfeb*$^{\Delta LysM}$.

753 **C.** Overlap of genes induced by PNU-282987 in *Tfeb*$^{f/f}$ compared to those
754 induced in *Tfeb*$^{\Delta LysM}$ BMDMs.

755 **D.** Differential gene expression of PNU-282987-treated (50 μM, 2 h) *Tfeb Tfe3*
756 double knockout (dKO) and WT RAW264.7 cells (FC ≥ 1.5; *P*adj. ≤ 0.01, 4 biological

757 replicates). Red indicates upregulated (UP), blue denotes downregulated (DOWN)
758 genes in dKO cells. Notable genes are highlighted.

759 **E.** GO-overrepresentation and KEGG pathway enrichment analysis for genes
760 upregulated in PNU-282987-treated WT RAW264.7 cells compared to dKO.

761

762 ***Figure 6. MCOLN1, Ca^{2+}, and PPP3/calcineurin are required for TFEB activation by***
763 ***PNU-282987***

764 **A-D.** Representative fluorescence micrographs of GFP-TFEB iBMDMs treated
765 with DMSO (negative control) (**A**), PNU-282987 (50 μM, 2 h) (**B**), BAPTA-AM (10 μM, 3
766 h pre-treatment) followed by addition of PNU-282987 (50 μM, 2 h) (**C**), or FK506 (5 μM,
767 6 h pre-treatment) followed by addition of PNU-282987 (50 μM, 2 h) (**D**).

768 **E.** Quantification of A-D. N/C ratio of GFP-TFEB (400 cells per condition, 3
769 biological replicates, ****$p \leq 0.0001$, one-way ANOVA followed by Tukey's post-hoc
770 test).

771 **F-L.** Representative fluorescence micrographs of GFP-TFEB iBMDMs treated
772 DMSO (negative control) (**F**), and with siRNA, Scrambled siRNA (Scr) (**G, J**) or directed
773 against *Ppp3cb* (**H**), *Ppp3r1* (**I**), and *Trpml1* (**K, L**) for 48 h prior to treatment with PNU-
774 282987 (50 μM, 2 h) or serum starvation (positive control, **J, L**).

775 **M.** Quantification of F-L. N/C ratio of GFP-TFEB (400 cells per condition, 3
776 biological replicates, ****$p \leq 0.0001$, one-way ANOVA followed by Tukey's post-hoc
777 test).

References

1. Perera, R. M., Di Malta, C., Ballabio, A. (2019) MiT/TFE Family of Transcription Factors, Lysosomes, and Cancer. Annu Rev Cancer Biol 3, 203-222.
2. O'Rourke, E. J. and Ruvkun, G. (2013) MXL-3 and HLH-30 transcriptionally link lipolysis and autophagy to nutrient availability. Nat Cell Biol 15, 668-76.
3. Settembre, C., De Cegli, R., Mansueto, G., Saha, P. K., Vetrini, F., Visvikis, O., Huynh, T., Carissimo, A., Palmer, D., Klisch, T. J., Wollenberg, A. C., Di Bernardo, D., Chan, L., Irazoqui, J. E., Ballabio, A. (2013) TFEB controls cellular lipid metabolism through a starvation-induced autoregulatory loop. Nat Cell Biol 15, 647-58.
4. Visvikis, O., Ihuegbu, N., Labed, S. A., Luhachack, L. G., Alves, A. F., Wollenberg, A. C., Stuart, L. M., Stormo, G. D., Irazoqui, J. E. (2014) Innate host defense requires TFEB-mediated transcription of cytoprotective and antimicrobial genes. Immunity 40, 896-909.
5. Pastore, N., Brady, O. A., Diab, H. I., Martina, J. A., Sun, L., Huynh, T., Lim, J. A., Zare, H., Raben, N., Ballabio, A., Puertollano, R. (2016) TFEB and TFE3 cooperate in the regulation of the innate immune response in activated macrophages. Autophagy 12, 1240-58.
6. Najibi, M., Honwad, H. H., Moreau, J. A., Becker, S. M., Irazoqui, J. E. (2022) A novel Nox/Phox-Cd38-Naadp-Tfeb axis important for macrophage activation during bacterial phagocytosis. Autophagy 18, 124-141.
7. Najibi, M., Labed, S. A., Visvikis, O., Irazoqui, J. E. (2016) An evolutionarily conserved PLC-PKD-TFEB pathway for host defense. Cell reports 15, 1728-1742.
8. Martina, J. A., Chen, Y., Gucek, M., Puertollano, R. (2012) MTORC1 functions as a transcriptional regulator of autophagy by preventing nuclear transport of TFEB. Autophagy 8, 903-14.
9. Pena-Llopis, S., Vega-Rubin-de-Celis, S., Schwartz, J. C., Wolff, N. C., Tran, T. A., Zou, L., Xie, X. J., Corey, D. R., Brugarolas, J. (2011) Regulation of TFEB and V-ATPases by mTORC1. Embo J 30, 3242-58.
10. Martina, J. A., Diab, H. I., Lishu, L., Jeong, A. L., Patange, S., Raben, N., Puertollano, R. (2014) The nutrient-responsive transcription factor TFE3 promotes autophagy, lysosomal biogenesis, and clearance of cellular debris. Sci Signal 7, ra9.
11. Roczniak-Ferguson, A., Petit, C. S., Froehlich, F., Qian, S., Ky, J., Angarola, B., Walther, T. C., Ferguson, S. M. (2012) The transcription factor TFEB links mTORC1 signaling to transcriptional control of lysosome homeostasis. Sci Signal 5, ra42.
12. Medina, D. L., Di Paola, S., Peluso, I., Armani, A., De Stefani, D., Venditti, R., Montefusco, S., Scotto-Rosato, A., Prezioso, C., Forrester, A., Settembre, C., Wang, W., Gao, Q., Xu, H., Sandri, M., Rizzuto, R., De Matteis, M. A., Ballabio, A.

(2015) Lysosomal calcium signalling regulates autophagy through calcineurin and TFEB. Nat Cell Biol 17, 288-99.

13. Gray, M. A., Choy, C. H., Dayam, R. M., Ospina-Escobar, E., Somerville, A., Xiao, X., Ferguson, S. M., Botelho, R. J. (2016) Phagocytosis enhances lysosomal and bactericidal properties by activating the transcription factor TFEB. Current Biology 26, 1955-1964.
14. Nabar, N. R., Heijjer, C. N., Shi, C.-S., Hwang, I.-Y., Ganesan, S., Karlsson, M. C., Kehrl, J. H. (2022) LRRK2 is required for CD38-mediated NAADP-Ca2+ signaling and the downstream activation of TFEB (transcription factor EB) in immune cells. Autophagy 18, 204-222.
15. Bertrand, D., Lee, C. H., Flood, D., Marger, F., Donnelly-Roberts, D. (2015) Therapeutic Potential of alpha7 Nicotinic Acetylcholine Receptors. Pharmacol Rev 67, 1025-73.
16. Borroni, V. and Barrantes, F. J. (2021) Homomeric and Heteromeric α7 Nicotinic Acetylcholine Receptors in Health and Some Central Nervous System Diseases. Membr 11, 664.
17. Tan, Y., Chu, Z., Shan, H., Zhangsun, D., Zhu, X., Luo, S. (2022) Inflammation regulation via an agonist and antagonists of α7 nicotinic acetylcholine receptors in RAW264. 7 macrophages. Marine Drugs 20, 200.
18. Richter, K. and Grau, V. (2023) Signaling of nicotinic acetylcholine receptors in mononuclear phagocytes. Pharmacol Res 191, 106727.
19. Kelly, M. J., Breathnach, C., Tracey, K. J., Donnelly, S. C. (2022) Manipulation of the inflammatory reflex as a therapeutic strategy. Cell Reports Medicine 3.
20. Halder, N. and Lal, G. (2021) Cholinergic system and its therapeutic importance in inflammation and autoimmunity. Frontiers in Immunology 12, 660342.
21. Li, B., Wu, J., Bao, J., Han, X., Shen, S., Ye, X., Dai, J., Wu, Z., Niu, M., He, Y., Ni, J., Wen, L., Wang, X., Hu, G. (2020) Activation of α7nACh receptor protects against acute pancreatitis through enhancing TFEB-regulated autophagy. Biochimica et Biophysica Acta (BBA) - Molecular Basis of Disease 1866, 165971.
22. Ito, T., Inden, M., Ueda, T., Asaka, Y., Kurita, H., Hozumi, I. (2020) The neuroprotective effects of activated α7 nicotinic acetylcholine receptor against mutant copper–zinc superoxide dismutase 1-mediated toxicity. Scientific Reports 10, 22157.
23. Hajos, M., Hurst, R., Hoffmann, W., Krause, M., Wall, T., Higdon, N., Groppi, V. (2005) The selective α7 nicotinic acetylcholine receptor agonist PNU-282987 [N-[(3R)-1-azabicyclo [2.2. 2] oct-3-yl]-4-chlorobenzamide hydrochloride] enhances GABAergic synaptic activity in brain slices and restores auditory gating deficits in anesthetized rats. Journal of Pharmacology and Experimental Therapeutics 312, 1213-1222.
24. Meltzer, L. T. and Rosecrans, J. A. (1988) Nicotine and arecoline as discriminative stimuli: involvement of a non-cholinergic mechanism for nicotine. Pharmacol Biochem Be 29, 587-93.
25. Maggi, L., Palma, E., Eusebi, F., Moretti, M., Balestra, B., Clementi, F., Gotti, C. (1999) Selective effects of a 4-oxystilbene derivative on wild and mutant neuronal chick alpha7 nicotinic receptor. Br J Pharmacol 126, 285-95.

26. Satoh, Y., Ishikawa, K., Oomori, Y., Yamano, M., Ono, K. (1989) Effects of cholecystokinin and carbamylcholine on Paneth cell secretion in mice: a comparison with pancreatic acinar cells. Anat Rec 225, 124-32.
27. Sardiello, M., Palmieri, M., Di Ronza, A., Medina, D. L., Valenza, M., Gennarino, V. A., Di Malta, C., Donaudy, F., Embrione, V., Polishchuk, R. S. (2009) A gene network regulating lysosomal biogenesis and function. Science 325, 473-477.
28. Settembre, C., Zoncu, R., Medina, D. L., Vetrini, F., Erdin, S., Erdin, S., Huynh, T., Ferron, M., Karsenty, G., Vellard, M. C., Facchinetti, V., Sabatini, D. M., Ballabio, A. (2012) A lysosome-to-nucleus signalling mechanism senses and regulates the lysosome via mTOR and TFEB. Embo J 31, 1095-108.
29. Raben, N. and Puertollano, R. (2016) TFEB and TFE3: Linking Lysosomes to Cellular Adaptation to Stress. Annu Rev Cell Dev Biol 32, 255-278.
30. Shao, Z., Li, Q., Wang, S., Chen, Z. (2019) Protective effects of PNU-282987 on sepsis-induced acute lung injury in mice. Molecular Medicine Reports 19, 3791-3798.
31. Kawashima, K., Yoshikawa, K., Fujii, Y. X., Moriwaki, Y., Misawa, H. (2007) Expression and function of genes encoding cholinergic components in murine immune cells. Life sciences 80, 2314-2319.
32. Lei, W., Zhao, C., Sun, J., Jin, Y., Duan, Z. (2022) Activation of α7nAChR preserves intestinal barrier integrity by enhancing the HO-1/STAT3 signaling to inhibit NF-κB activation in mice. Biomedicine & Pharmacotherapy 149, 112733.
33. Chen, Y., Lian, P., Peng, Z., Wazir, J., Ma, C., Wei, L., Li, L., Liu, J., Zhao, C., Pu, W. (2022) Alpha-7 nicotinic acetylcholine receptor agonist alleviates psoriasis-like inflammation through inhibition of the STAT3 and NF-κB signaling pathway. Cell Death Discovery 8, 141.
34. Herber, D. L., Severance, E. G., Cuevas, J., Morgan, D., Gordon, M. N. (2004) Biochemical and Histochemical Evidence of Nonspecific Binding of α7nAChR Antibodies to Mouse Brain Tissue. J Histochem Cytochem 52, 1367-1375.
35. Moser, N., Mechawar, N., Jones, I., Gochberg-Sarver, A., Orr-Urtreger, A., Plomann, M., Salas, R., Molles, B., Marubio, L., Roth, U., Maskos, U., Winzer-Serhan, U., Bourgeois, J. P., Sourd, A. M. L., Biasi, M. D., Schröder, H., Lindstrom, J., Maelicke, A., Changeux, J. P., Wevers, A. (2007) Evaluating the suitability of nicotinic acetylcholine receptor antibodies for standard immunodetection procedures. J Neurochem 102, 479-492.
36. Matteoli, G., Gomez-Pinilla, P. J., Nemethova, A., Di Giovangiulio, M., Cailotto, C., van Bree, S. H., Michel, K., Tracey, K. J., Schemann, M., Boesmans, W., Vanden Berghe, P., Boeckxstaens, G. E. (2014) A distinct vagal anti-inflammatory pathway modulates intestinal muscularis resident macrophages independent of the spleen. Gut 63, 938-48.
37. Orr-Urtreger, A., Göldner, F. M., Saeki, M., Lorenzo, I., Goldberg, L., De Biasi, M., Dani, J. A., Patrick, J. W., Beaudet, A. L. (1997) Mice deficient in the α7 neuronal nicotinic acetylcholine receptor lack α-bungarotoxin binding sites and hippocampal fast nicotinic currents. Journal of Neuroscience 17, 9165-9171.
38. Carey, K., Paulus, G., Wang, L., Balce, D., Luo, J., Bergman, P., Ferder, I., Kong, L., Renaud, N., Singh, S. (2020) TFEB transcriptional responses reveal negative feedback by BHLHE40 and BHLHE41. Cell Rep 33: 108371.

39. Xu, W.-D., Li, R., Huang, A.-F. (2022) Role of TL1A in inflammatory autoimmune diseases: a comprehensive review. Frontiers in Immunology 13, 891328.
40. Martina, J. A., Diab, H. I., Lishu, L., Jeong-A, L., Patange, S., Raben, N., Puertollano, R. (2014) The nutrient-responsive transcription factor TFE3 promotes autophagy, lysosomal biogenesis, and clearance of cellular debris. Science signaling 7, ra9-ra9.
41. Pastore, N., Brady, O. A., Diab, H. I., Martina, J. A., Sun, L., Huynh, T., Lim, J.-A., Zare, H., Raben, N., Ballabio, A. (2016) TFEB and TFE3 cooperate in the regulation of the innate immune response in activated macrophages. Autophagy 12, 1240-1258.
42. Liu, J., Farmer Jr, J. D., Lane, W. S., Friedman, J., Weissman, I., Schreiber, S. L. (1991) Calcineurin is a common target of cyclophilin-cyclosporin A and FKBP-FK506 complexes. Cell 66, 807-815.
43. Najibi, M., Labed, S. A., Visvikis, O., Irazoqui, J. E. (2016) An Evolutionarily Conserved PLC-PKD-TFEB Pathway for Host Defense. Cell Rep 15, 1728-42.
44. LaValle, C. R., Bravo-Altamirano, K., Giridhar, K. V., Chen, J., Sharlow, E., Lazo, J. S., Wipf, P., Wang, Q. J. (2010) Novel protein kinase D inhibitors cause potent arrest in prostate cancer cell growth and motility. BMC chemical biology 10, 1-16.
45. Zhang, X., Cheng, X., Yu, L., Yang, J., Calvo, R., Patnaik, S., Hu, X., Gao, Q., Yang, M., Lawas, M. (2016) MCOLN1 is a ROS sensor in lysosomes that regulates autophagy. Nature communications 7, 12109.
46. Martina, J. A. and Puertollano, R. (2018) Protein phosphatase 2A stimulates activation of TFEB and TFE3 transcription factors in response to oxidative stress. Journal of Biological Chemistry 293, 12525-12534.
47. Samie, M., Wang, X., Zhang, X., Goschka, A., Li, X., Cheng, X., Gregg, E., Azar, M., Zhuo, Y., Garrity, A. G., Gao, Q., Slaugenhaupt, S., Pickel, J., Zolov, S. N., Weisman, L. S., Lenk, G. M., Titus, S., Bryant-Genevier, M., Southall, N., Juan, M., Ferrer, M., Xu, H. (2013) A TRP channel in the lysosome regulates large particle phagocytosis via focal exocytosis. Dev Cell 26, 511-24.
48. Ginhoux, F. and Guilliams, M. (2016) Tissue-Resident Macrophage Ontogeny and Homeostasis. Immunity 44, 439-449.
49. Wynn, T. A., Chawla, A., Pollard, J. W. (2013) Macrophage biology in development, homeostasis and disease. Nature 496, 445-455.
50. Mosser, D. M. and Gonçalves, R. (2015) Activation of Murine Macrophages. Current Protocols in Immunology 111, 14.2.1-14.2.10.
51. Mosser, D. M. and Edwards, J. P. (2008) Exploring the full spectrum of macrophage activation. Nat Rev Immunol 8, 958-69.
52. Ginhoux, F. and Jung, S. (2014) Monocytes and macrophages: developmental pathways and tissue homeostasis. Nat Rev Immunol 14, 392-404.
53. Murray, P. J. and Wynn, T. A. (2011) Protective and pathogenic functions of macrophage subsets. Nat Rev Immunol 11, 723-37.
54. Gordon, S. and Martinez, F. O. (2010) Alternative activation of macrophages: mechanism and functions. Immunity 32, 593-604.
55. Tan, Y., Chu, Z., Shan, H., Zhangsun, D., Zhu, X., Luo, S. (2022) Inflammation Regulation via an Agonist and Antagonists of alpha7 Nicotinic Acetylcholine Receptors in RAW264.7 Macrophages. Mar Drugs 20, 200.

957 56. Garg, B. K. and Loring, R. H. (2019) GTS-21 has cell-specific anti-inflammatory
958 effects independent of α7 nicotinic acetylcholine receptors. PLOS ONE 14,
959 e0214942.
960 57. Tsoyi, K., Jang, H. J., Kim, J. W., Chang, H. K., Lee, Y. S., Pae, H.-O., Kim, H. J.,
961 Seo, H. G., Lee, J. H., Chung, H.-T. (2011) Stimulation of alpha7 nicotinic
962 acetylcholine receptor by nicotine attenuates inflammatory response in
963 macrophages and improves survival in experimental model of sepsis through
964 heme oxygenase-1 induction. Antioxidants & redox signaling 14, 2057-2070.
965 58. Lau, P. P., Li, L., Merched, A. J., Zhang, A. L., Ko, K. W., Chan, L. (2006) Nicotine
966 induces proinflammatory responses in macrophages and the aorta leading to
967 acceleration of atherosclerosis in low-density lipoprotein receptor(-/-) mice.
968 Arterioscler Thromb Vasc Biol 26, 143-9.
969 59. Hamano, R., Takahashi, H. K., Iwagaki, H., Yoshino, T., Nishibori, M., Tanaka, N.
970 (2006) Stimulation of alpha7 nicotinic acetylcholine receptor inhibits CD14 and
971 the toll-like receptor 4 expression in human monocytes. Shock 26, 358-64.
972 60. Takahashi, H. K., Iwagaki, H., Hamano, R., Yoshino, T., Tanaka, N., Nishibori, M.
973 (2006) Effect of nicotine on IL-18-initiated immune response in human
974 monocytes. J Leukocyte Biol 80, 1388-94.
975 61. Mao, J., Liu, J., Pang, X., Li, M., Song, J., Han, C., Wu, D., Wang, S. (2012)
976 Nicotine induces the expression of C-reactive protein via MAPK-dependent
977 signal pathway in U937 macrophages. Mol Cells 34, 457-61.
978 62. Hung, M. Y., Wu, Y. H., Bamodu, O. A., Chen, X., Lin, Y. K., Hu, P., Chang, N. C.,
979 Pang, J. S., Yeh, C. T. (2018) Activation of the monocytic alpha7 nicotinic
980 acetylcholine receptor modulates oxidative stress and inflammation-associated
981 development of coronary artery spasm via a p38 MAP-kinase signaling-
982 dependent pathway. Free Radic Biol Med 120, 266-276.
983 63. Suzuki, T., Hide, I., Matsubara, A., Hama, C., Harada, K., Miyano, K., Andra, M.,
984 Matsubayashi, H., Sakai, N., Kohsaka, S., Inoue, K., Nakata, Y. (2006) Microglial
985 alpha7 nicotinic acetylcholine receptors drive a phospholipase C/IP3 pathway
986 and modulate the cell activation toward a neuroprotective role. J Neurosci Res
987 83, 1461-70.
988 64. Siniavin, A. E., Streltsova, M. A., Kudryavtsev, D. S., Shelukhina, I. V., Utkin, Y.
989 N., Tsetlin, V. I. (2020) Activation of alpha7 Nicotinic Acetylcholine Receptor
990 Upregulates HLA-DR and Macrophage Receptors: Potential Role in Adaptive
991 Immunity and in Preventing Immunosuppression. Biomolecules 10, 507.
992 65. Anderson, P. (2008) Post-transcriptional control of cytokine production. Nature
993 Immunology 9, 353-359.
994 66. Piccirillo, C. A., Bjur, E., Topisirovic, I., Sonenberg, N., Larsson, O. (2014)
995 Translational control of immune responses: from transcripts to translatomes.
996 Nature Immunology 15, 503-511.
997 67. Sharma, B. R. and Kanneganti, T. D. (2021) NLRP3 inflammasome in cancer and
998 metabolic diseases. Nat Immunol 22, 550-559.
999 68. Rathinam, V. A. K., Zhao, Y., Shao, F. (2019) Innate immunity to intracellular LPS.
1000 Nat Immunol 20, 527-533.

69. Settembre, C., Di Malta, C., Polito, V. A., Arencibia, M. G., Vetrini, F., Erdin, S., Erdin, S. U., Huynh, T., Medina, D., Colella, P. (2011) TFEB links autophagy to lysosomal biogenesis. science 332, 1429-1433.
70. McQuin, C., Goodman, A., Chernyshev, V., Kamentsky, L., Cimini, B. A., Karhohs, K. W., Doan, M., Ding, L., Rafelski, S. M., Thirstrup, D. (2018) CellProfiler 3.0: Next-generation image processing for biology. PLoS biology 16, e2005970.
71. Yukselen, O., Turkyilmaz, O., Ozturk, A. R., Garber, M., Kucukural, A. (2020) DolphinNext: a distributed data processing platform for high throughput genomics. BMC genomics 21, 1-16.
72. Kucukural, A., Yukselen, O., Ozata, D. M., Moore, M. J., Garber, M. (2019) DEBrowser: interactive differential expression analysis and visualization tool for count data. Bmc Genomics 20, 6.
73. Reimand, J., Isserlin, R., Voisin, V., Kucera, M., Tannus-Lopes, C., Rostamianfar, A., Wadi, L., Meyer, M., Wong, J., Xu, C., Merico, D., Bader, G. D. (2019) Pathway enrichment analysis and visualization of omics data using g:Profiler, GSEA, Cytoscape and EnrichmentMap. Nat Protoc 14, 482-517.
74. Evangelista, J. E., Xie, Z., Marino, G. B., Nguyen, N., Clarke, Daniel J. B., Ma'ayan, A. (2023) Enrichr-KG: bridging enrichment analysis across multiple libraries. Nucleic Acids Research 51, W168-W179.
75. Hulsen, T. (2022) DeepVenn--a web application for the creation of area-proportional Venn diagrams using the deep learning framework Tensorflow. js. arXiv preprint arXiv:2210.04597.
76. Koscsó, B., Gowda, K., Schell, T. D., Bogunovic, M. (2015) Purification of dendritic cell and macrophage subsets from the normal mouse small intestine. Journal of immunological methods 421, 1-13.
77. Koscsó, B. and Bogunovic, M. (2016) Analysis and purification of mouse intestinal dendritic cell and macrophage subsets by flow cytometry. Current Protocols in Immunology 114, 14.39. 1-14.39. 14.

FIGURE 1

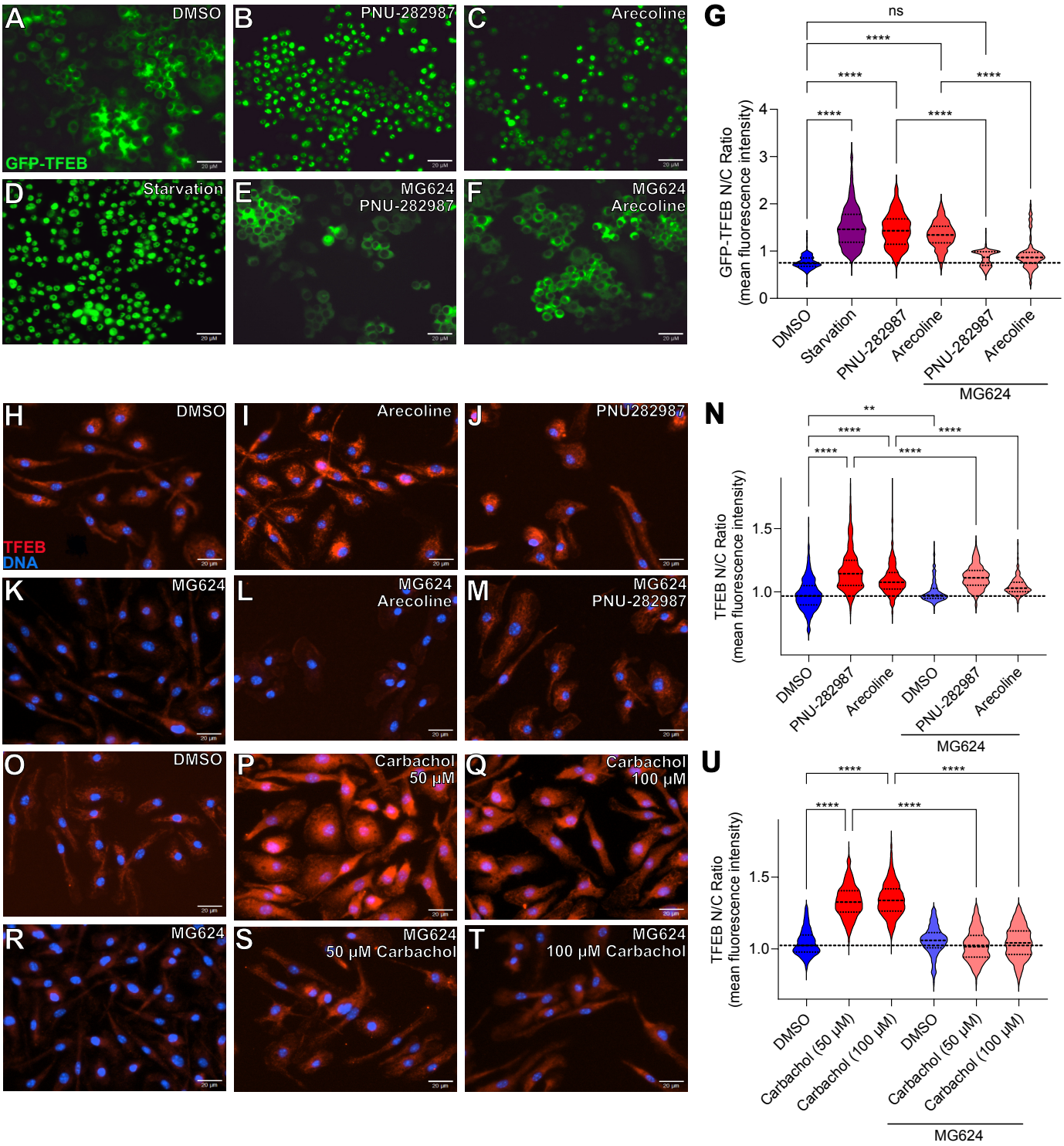
A
DMSO
GFP-TFEB
B
PNU-282987
C
Arecoline
D
Starvation
E
MG624
PNU-282987
F
MG624
Arecoline
G
ns
****
GFP-TFEB N/C Ratio
(mean fluorescence intensity)
DMSO
Starvation
PNU-282987
Arecoline
PNU-282987
Arecoline
MG624
H
DMSO
TFEB
DNA
I
Arecoline
J
PNU282987
K
MG624
L
MG624
Arecoline
M
MG624
PNU-282987
N
**
****
TFEB N/C Ratio
(mean fluorescence intensity)
DMSO
PNU-282987
Arecoline
DMSO
PNU-282987
Arecoline
MG624
O
DMSO
P
Carbachol
50 µM
Q
Carbachol
100 µM
R
MG624
S
MG624
50 µM Carbachol
T
MG624
100 µM Carbachol
U
****
TFEB N/C Ratio
(mean fluorescence intensity)
DMSO
Carbachol (50 µM)
Carbachol (100 µM)
DMSO
Carbachol (50 µM)
Carbachol (100 µM)
MG624

FIGURE 2

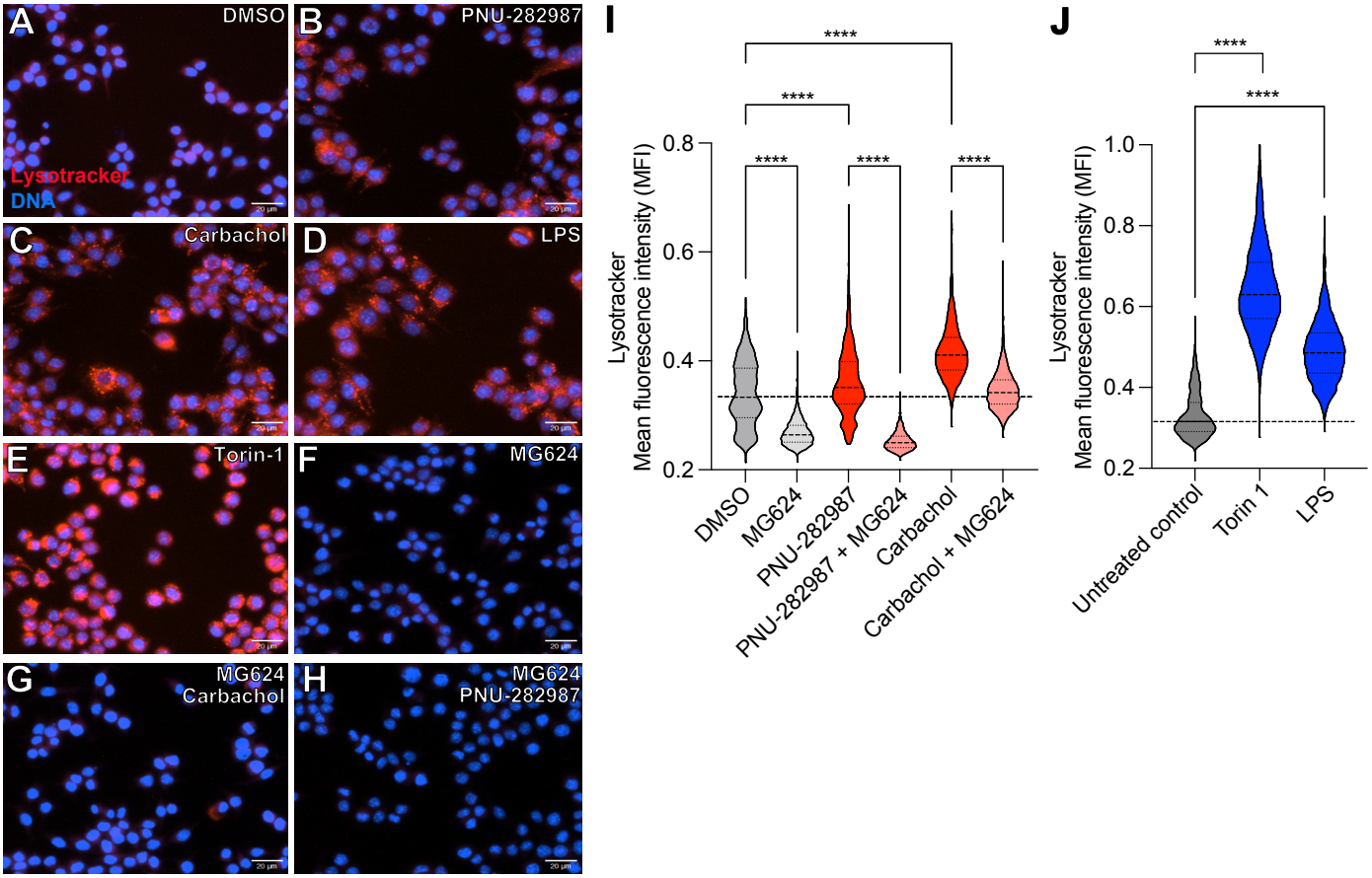
A
DMSO
Lysotracker
DNA
B
PNU-282987
C
Carbachol
D
LPS
E
Torin-1
F
MG624
G
MG624
Carbachol
H
MG624
PNU-282987
I
Lysotracker
Mean fluorescence intensity (MFI)
0.8
0.6
0.4
0.2
****
DMSO
MG624
PNU-282987
PNU-282987 + MG624
Carbachol
Carbachol + MG624
J
Lysotracker
Mean fluorescence intensity (MFI)
1.0
0.8
0.6
0.4
0.2
Untreated control
Torin 1
LPS

FIGURE 3

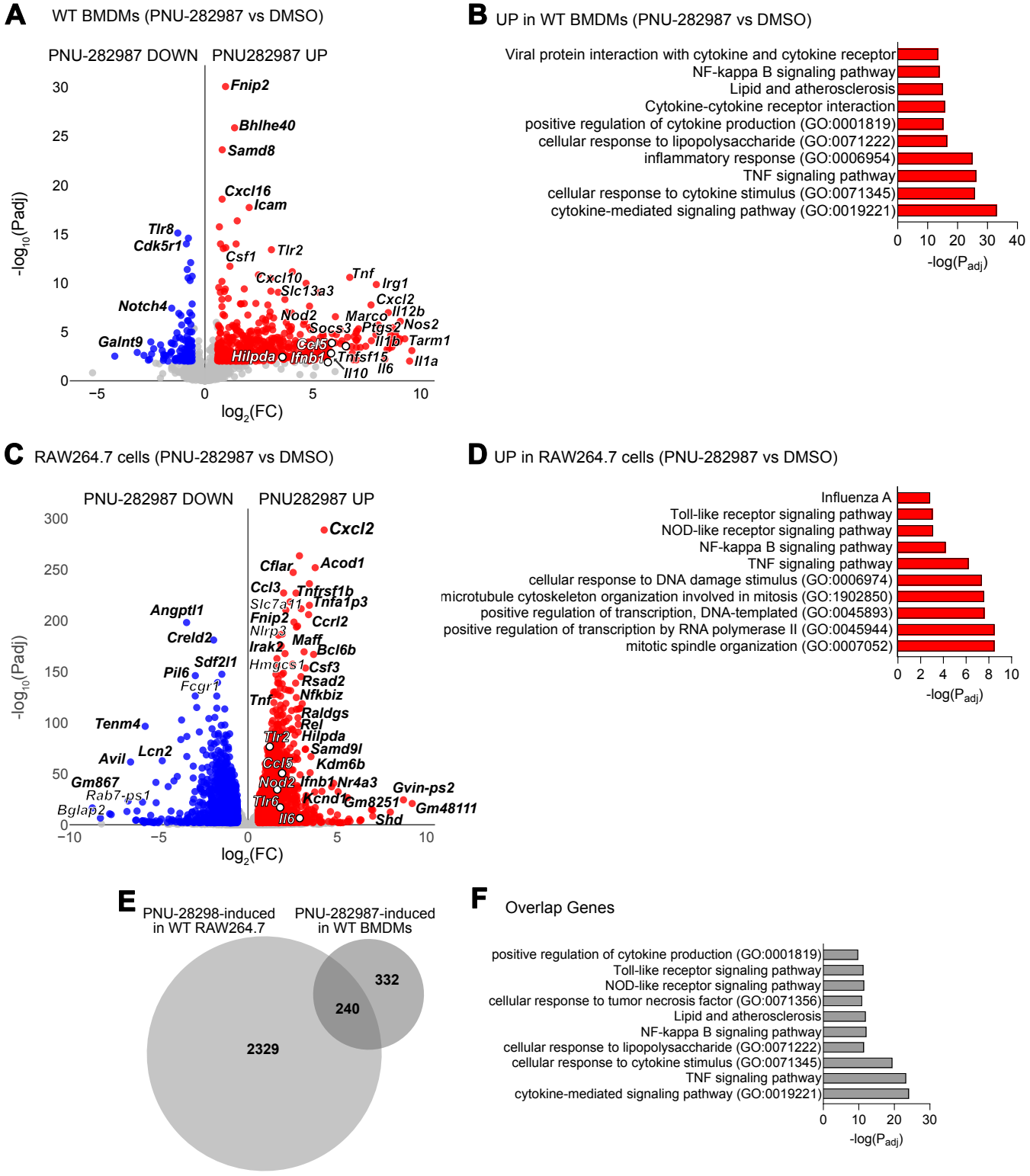
A
WT BMDMs (PNU-282987 vs DMSO)
PNU-282987 DOWN
PNU282987 UP
-log10(Padj)
log2(FC)
Fnip2
Bhlhe40
Samd8
Cxcl16
Icam
Tlr8
Cdk5r1
Csf1
Tlr2
Cxcl10
Slc13a3
Tnf
Irg1
Cxcl2
Il12b
Notch4
Nod2
Marco
Socs3
Ptgs2
Nos2
Il1b
Tarm1
Galnt9
Ccl5
Hilpda
Ifnb1
Tnfsf15
Il10
Il6
Il1a
B
UP in WT BMDMs (PNU-282987 vs DMSO)
Viral protein interaction with cytokine and cytokine receptor
NF-kappa B signaling pathway
Lipid and atherosclerosis
Cytokine-cytokine receptor interaction
positive regulation of cytokine production (GO:0001819)
cellular response to lipopolysaccharide (GO:0071222)
inflammatory response (GO:0006954)
TNF signaling pathway
cellular response to cytokine stimulus (GO:0071345)
cytokine-mediated signaling pathway (GO:0019221)
-log(Padj)
C
RAW264.7 cells (PNU-282987 vs DMSO)
PNU-282987 DOWN
PNU282987 UP
-log10(Padj)
log2(FC)
Cxcl2
Cflar
Acod1
Ccl3
Tnfrsf1b
Slc7a11
Tnfa1p3
Angptl1
Fnip2
Ccrl2
Nlrp3
Creld2
Maff
Irak2
Bcl6b
Sdf2l1
Hmgcs1
Csf3
Pil6
Fcgr1
Rsad2
Nfkbiz
Tnf
Raldgs
Rel
Tenm4
Tlr2
Hilpda
Samd9l
Avil
Lcn2
Ccl5
Kdm6b
Gm867
Nod2
Ifnb1
Nr4a3
Gvin-ps2
Rab7-ps1
Kcnd1
Gm8251
Gm48111
Bglap2
Tlr6
Il6
Shd
D
UP in RAW264.7 cells (PNU-282987 vs DMSO)
Influenza A
Toll-like receptor signaling pathway
NOD-like receptor signaling pathway
NF-kappa B signaling pathway
TNF signaling pathway
cellular response to DNA damage stimulus (GO:0006974)
microtubule cytoskeleton organization involved in mitosis (GO:1902850)
positive regulation of transcription, DNA-templated (GO:0045893)
positive regulation of transcription by RNA polymerase II (GO:0045944)
mitotic spindle organization (GO:0007052)
-log(Padj)
E
PNU-28298-induced in WT RAW264.7
PNU-282987-induced in WT BMDMs
332
240
2329
F
Overlap Genes
positive regulation of cytokine production (GO:0001819)
Toll-like receptor signaling pathway
NOD-like receptor signaling pathway
cellular response to tumor necrosis factor (GO:0071356)
Lipid and atherosclerosis
NF-kappa B signaling pathway
cellular response to lipopolysaccharide (GO:0071222)
cellular response to cytokine stimulus (GO:0071345)
TNF signaling pathway
cytokine-mediated signaling pathway (GO:0019221)
-log(Padj)

FIGURE 4

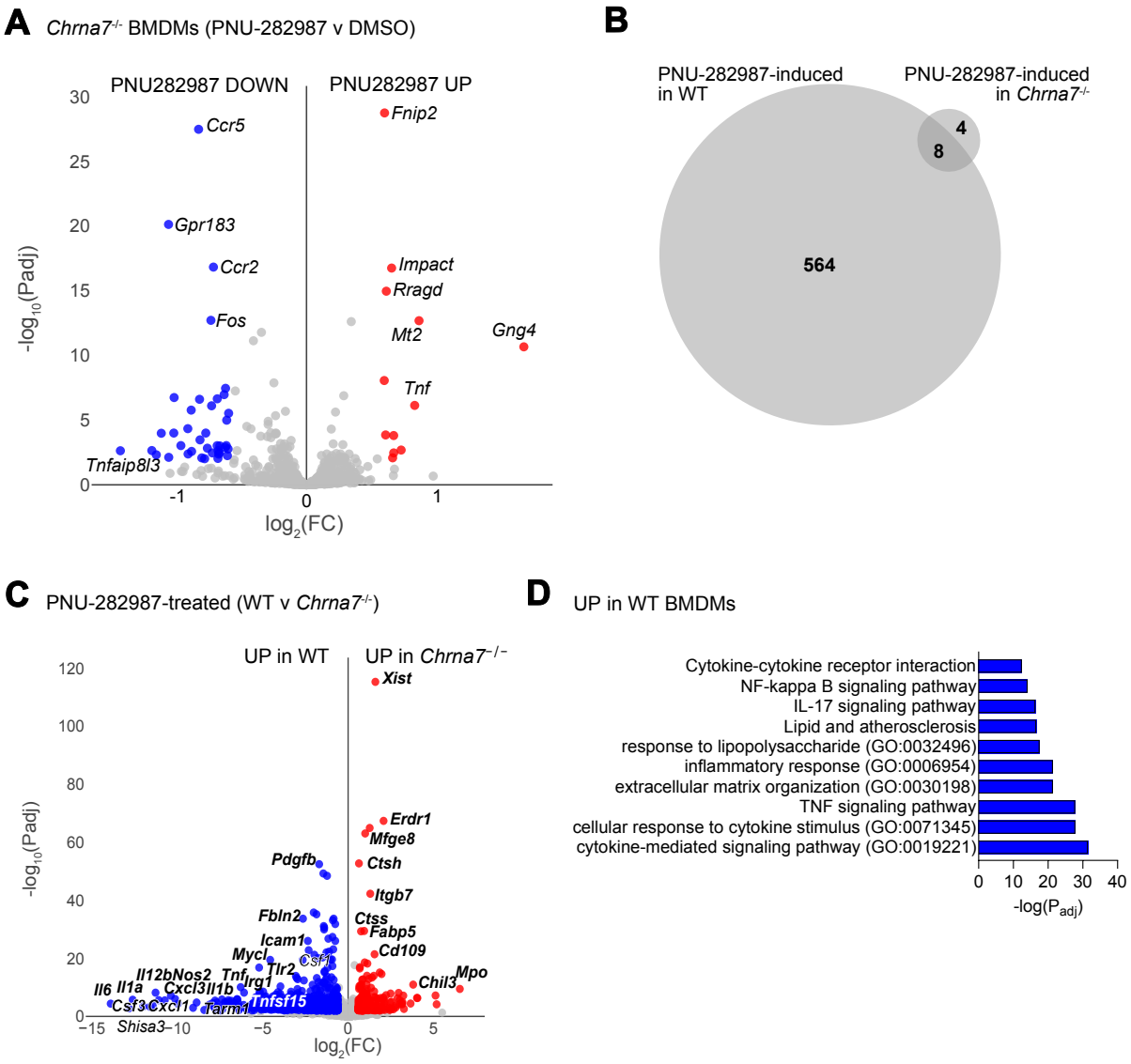
A
Chrna7-/- BMDMs (PNU-282987 v DMSO)
PNU282987 DOWN
PNU282987 UP
Ccr5
Gpr183
Ccr2
Fos
Tnfaip8l3
Fnip2
Impact
Rragd
Mt2
Gng4
Tnf
-log10(Padj)
log2(FC)
B
PNU-282987-induced in WT
PNU-282987-induced in Chrna7-/-
4
8
564
C
PNU-282987-treated (WT v Chrna7-/-)
UP in WT
UP in Chrna7-/-
Xist
Erdr1
Mfge8
Ctsh
Itgb7
Ctss
Fabp5
Cd109
Mpo
Chil3
Pdgfb
Fbln2
Icam1
Mycl
Csf1
Tlr2
Il12bNos2
Tnf
Irg1
Il6
Il1a
Cxcl3
Il1b
Csf3
Cxcl1
Tarm1
Tnfsf15
Shisa3
D
UP in WT BMDMs
Cytokine-cytokine receptor interaction
NF-kappa B signaling pathway
IL-17 signaling pathway
Lipid and atherosclerosis
response to lipopolysaccharide (GO:0032496)
inflammatory response (GO:0006954)
extracellular matrix organization (GO:0030198)
TNF signaling pathway
cellular response to cytokine stimulus (GO:0071345)
cytokine-mediated signaling pathway (GO:0019221)
-log(Padj)

FIGURE 5

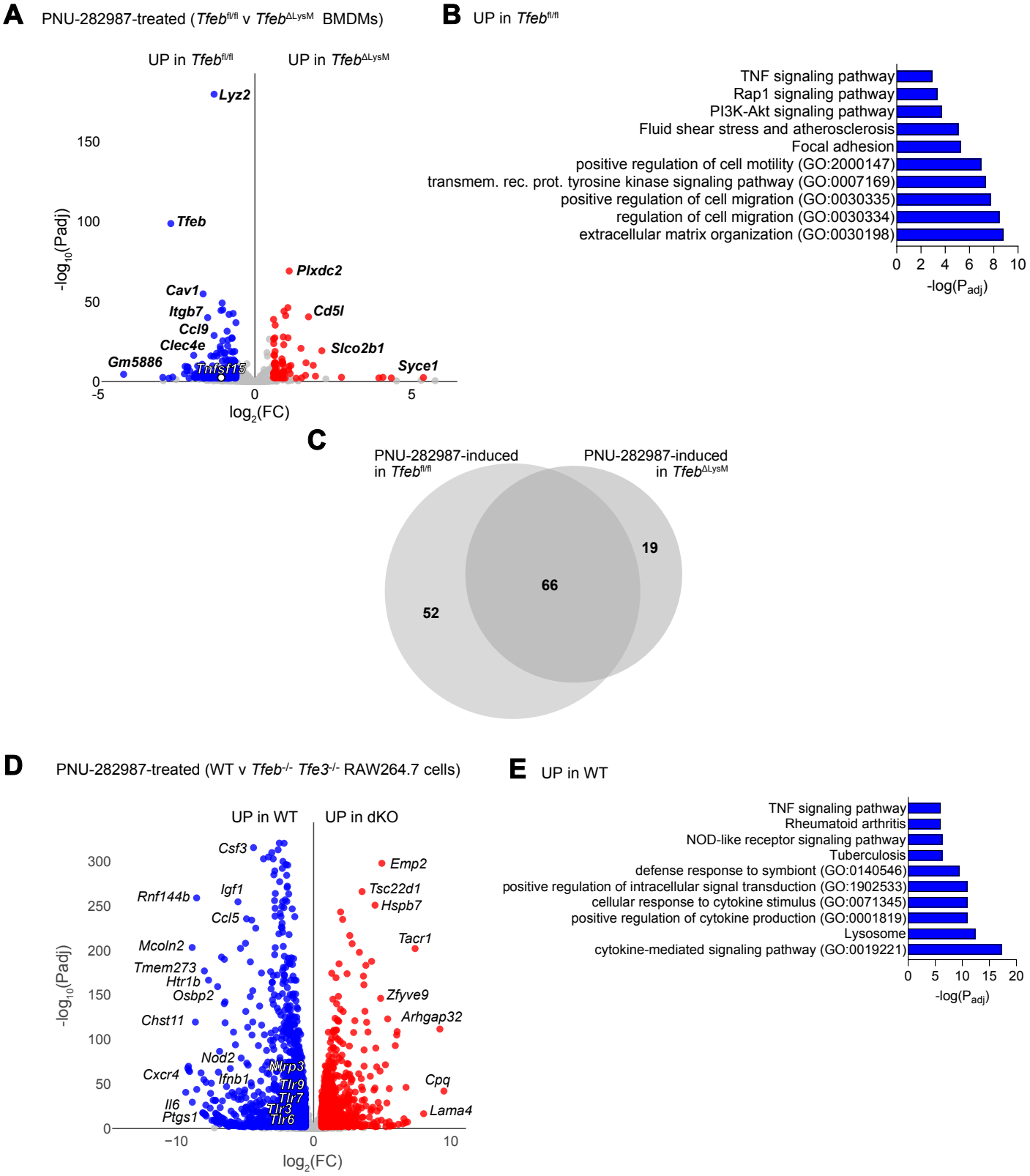
A
PNU-282987-treated (Tfeb fl/fl v Tfeb ΔLysM BMDMs)
UP in Tfeb fl/fl
UP in Tfeb ΔLysM
Lyz2
Tfeb
Cav1
Itgb7
Ccl9
Clec4e
Gm5886
Tnfsf15
Plxdc2
Cd5l
Slco2b1
Syce1
-log10(Padj)
log2(FC)
B
UP in Tfeb fl/fl
TNF signaling pathway
Rap1 signaling pathway
PI3K-Akt signaling pathway
Fluid shear stress and atherosclerosis
Focal adhesion
positive regulation of cell motility (GO:2000147)
transmem. rec. prot. tyrosine kinase signaling pathway (GO:0007169)
positive regulation of cell migration (GO:0030335)
regulation of cell migration (GO:0030334)
extracellular matrix organization (GO:0030198)
-log(Padj)
C
PNU-282987-induced in Tfeb fl/fl
PNU-282987-induced in Tfeb ΔLysM
52
66
19
D
PNU-282987-treated (WT v Tfeb-/- Tfe3-/- RAW264.7 cells)
UP in WT
UP in dKO
Csf3
Rnf144b
Igf1
Ccl5
Mcoln2
Tmem273
Htr1b
Osbp2
Chst11
Nod2
Cxcr4
Ifnb1
Il6
Ptgs1
Nlrp3
Tlr9
Tlr7
Tlr3
Tlr6
Emp2
Tsc22d1
Hspb7
Tacr1
Zfyve9
Arhgap32
Cpq
Lama4
-log10(Padj)
log2(FC)
E
UP in WT
TNF signaling pathway
Rheumatoid arthritis
NOD-like receptor signaling pathway
Tuberculosis
defense response to symbiont (GO:0140546)
positive regulation of intracellular signal transduction (GO:1902533)
cellular response to cytokine stimulus (GO:0071345)
positive regulation of cytokine production (GO:0001819)
Lysosome
cytokine-mediated signaling pathway (GO:0019221)
-log(Padj)

FIGURE 6

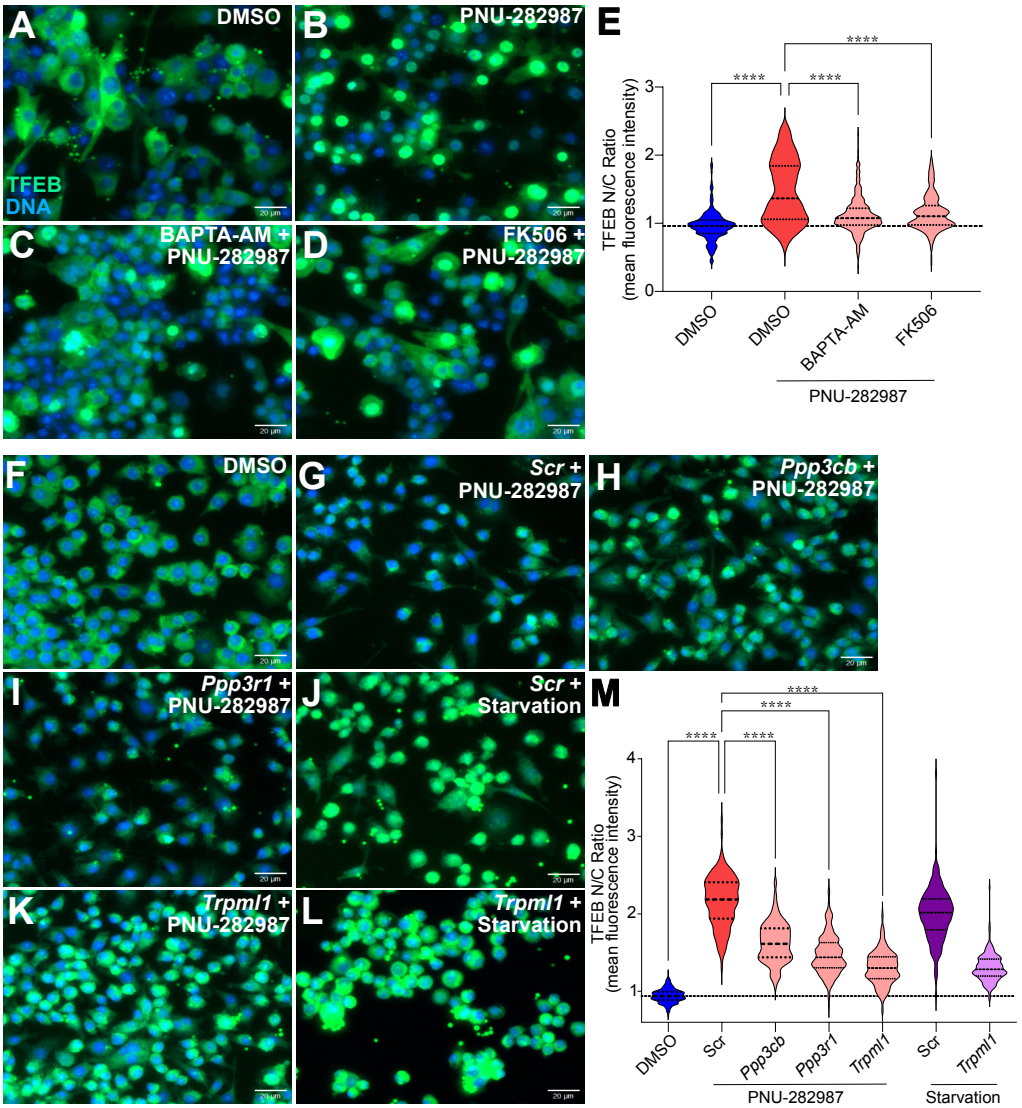
A
DMSO
TFEB
DNA
B
PNU-282987
C
BAPTA-AM +
PNU-282987
D
FK506 +
PNU-282987
E
TFEB N/C Ratio
(mean fluorescence intensity)
****
DMSO
DMSO
BAPTA-AM
FK506
PNU-282987
F
DMSO
G
Scr +
PNU-282987
H
Ppp3cb +
PNU-282987
I
Ppp3r1 +
PNU-282987
J
Scr +
Starvation
K
Trpml1 +
PNU-282987
L
Trpml1 +
Starvation
M
TFEB N/C Ratio
(mean fluorescence intensity)
DMSO
Scr
Ppp3cb
Ppp3r1
Trpml1
Scr
Trpml1
PNU-282987
Starvation